# Magel: An Advanced Partially Reusable Launch Architecture Concept

Stephen Steffes

AE8900 Special Project Report
December 5, 2003

School of Aerospace Engineering
Space System Design Laboratory
Georgia Institute of Technology
Atlanta, Georgia 30332-0150
Advisor: Dr. John R. Olds

# Table of Contents

# List of Figures

# List of Tables

# Abstract

Magel is an advanced partially reusable launch architecture which uses two large magnetically repelled superconducting rings as the first stage system and a liquid expendable rocket as the upper stage. At launch, the two rings lay on top of each other with the second stage suspended in the center, attached to the upper ring by cables. When the rings are fully charged the upper ring is released, dragging the second stage with it. Before the net upward force on the vehicle vanishes, the second stage is released and sent to orbit while the ring slowly falls back to Earth.

This architecture is studied in an attempt to drastically reduce launch costs. The first stage is fully reusable and must be refueled before every launch. The only resources used are the upper stage rocket and the attitude control propellant. A full launch vehicle analysis is presented including an analysis of the system's feasibility and viability considering various technology tradeoffs.

The baseline vehicle was found to be not feasible or viable even with infused technologies. The first stage ring is 6.6 km in diameter and 3.3 km high with a total dry weight of 15e6 lbs (6.8e6 kg). The cross section of the first stage ring is 2.2 m wide by 5.4 m high. Assuming a 56,900 lbs (25,800 kg) payload, 20 flights/year and a program length of 30 years, the total cost per pound to a 100 by 100 nmi 28.5° orbit is $35,500 FY2003/lbs.

# List of Acronyms

| | |
|---|---|
| $\alpha$ | Angle of Attack |
| AATe | Architecture Assessment Tool-enhanced |
| ADCS | Attitude Determination and Control System |
| $B_c$ | Critical Magnetic Field |
| BSCCO | (Bi,Pb)2Sr2Ca2Cu3Ox |
| CAD | Computer Aided Design |
| CBAero | Configuration Based Aerodynamics |
| CDF | Cumulative Distribution Function |
| CDt | Coefficient of Total Drag |
| CLt | Coefficient of Total Lift |
| D4H | Delta 4 Heavy |
| DDT&E | Design, Development, Testing and Evaluation |
| DSM | Design Structure Matrix |
| $I_g$ | Ground Ring Current |
| $I_{sp}$ | Specific Impulse |
| IVHM | Internal Vehicle Health Monitoring |
| $J_c$ | Critical Current Density |
| KSC | Kennedy Space Center |
| LCC | Life Cycle Cost |
| LHe | Liquid Helium |
| M | Mach |
| MCS | Monte Carlo Simulation |
| MER | Mass Estimating Relationship |
| MFBF | Mean Flights Between Failures |
| MTBF | Mean Time Between Failures |
| NAFCOM | NASA-Air Force Cost Model |
| Pro/E | Pro/ENGINEER |
| q | Dynamic Pressure |
| RLV | Reusable Launch Vehicle |
| ROSETTA | Reduced-Order Simulation for Evaluating Technologies and Transportation Architectures |
| RSE | Response Surface Equation |
| SC | Superconducting |
| SSME | Space Shuttle Main Engine |
| $T_c$ | Critical Temperature |
| TFU | Theoretical First Unit |
| TPS | Thermal Protection System |

# Introduction

The high cost of access to space has greatly burdened advancements in space technology and exploration. Lowering this cost is an important step towards making space access more affordable. One way to drastically reduce launch costs is to use a new, advanced launch architecture. The use of magnetic fields to push a payload into space is one promising architecture type. Some designs that have explored this notion (Maglifter [1] and StarTram[4]) have produced optimistic results. Magel is another such architecture that utilizes magnetic fields and may hold the key for low cost access to space.

Magel has most of the same requirements as a Delta 4 Heavy (D4H). It is a cargo only vehicle capable of carrying 25,800 kg (56,900 lbs) to a 28.5°, 100 nmi by 100 nmi orbit around Earth. It launches from a ground facility located at least 17.5 km East of Kennedy Space Center (KSC) in the Atlantic Ocean.

Magel is an advanced partially reusable launch architecture which uses two large magnetically repelled superconducting (SC) rings as the first stage system and a liquid expendable rocket as the upper stage. At launch, the two rings lay on top of each other with the second stage suspended in the center, attached to the upper ring by cables. When the rings are fully charged the upper ring is released, towing the second stage with it. Before the net upward force on the vehicle vanishes, the upper stage is ignited and released while the ring slowly falls back to Earth. Variations of this architecture will be studied in an attempt to drastically reduce launch costs compared to the D4H. A full disciplinary analysis of the vehicle is presented, as well as Monte Carlo simulations for the systems feasibility and viability.

# Electrodynamics

Currently there are only a handful of launch architectures that rely heavily on electrodynamics. StarTram uses a magnetically levitated evacuated launch tube. In this architecture, the space vehicle enters the beginning of the tube on the ground, is accelerated to near orbital velocity within the tube and exits the end of the tube at an altitude of ~20 km. This in analogous to a projectile traveling through a rail gun and

uses some of the same principles. Maglifter is a launch assist architecture that pushes a space vehicle along a track using magnetic fields before the vehicle takes off and flies into space. This is analogous to a bullet train.

Magel uses two physical dipoles for its first stage. The dipole moments are oriented in opposite directions so that they repel from one another. One dipole is stationary, on the ground, while the other is repelled upwards, towing the second stage rocket. To understand how this system works, basic electrodynamics must be discussed.

All magnetic fields are produced by electric currents. For a steady line current, the magnetic field is given by the Biot-Savart law:

$$\vec{B}(\vec{r}) = \frac{\mu_0}{4\pi} I \int \frac{d\vec{l} \times \hat{\mathfrak{R}}}{\mathfrak{R}^2}$$

where

$$\mu_0 = 4\pi \times 10^{-7} \, \text{N/A}^2$$

is the permeability of free space, I is a steady line current, $d\vec{l}$ is a differential element of length along the current and $\vec{\mathfrak{R}}$ is the vector from $d\vec{l}$ to $\vec{r}$ (Figure 1). Integration is along the current path in the direction of positive current flow. For a straight steady line current, the magnetic field direction can be found using the right hand rule. If the right hand's thumb points in the direction of the current then the magnetic field wraps around the current in the direction of the fingers (Figure 1).
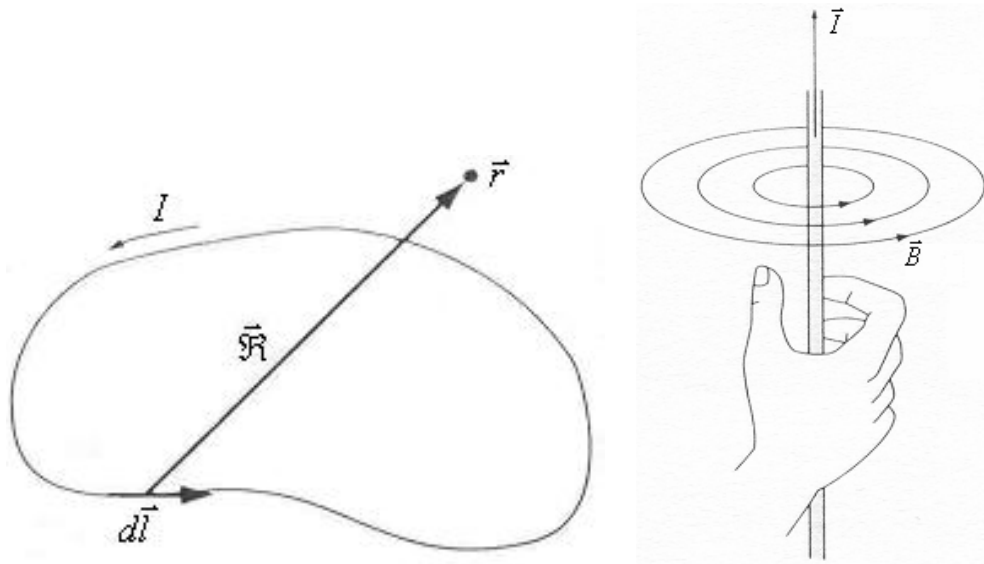


**Figure 1: Geometry of the Biot-Savart law (left) [2], an illustration of the right hand rule (right) [2].**

When a particle with charge Q moves through a magnetic field, a force is applied to the particle according to the Lorentz force law:

$$\vec{F} = Q(\vec{v} \times \vec{B})$$

where $\vec{F}$ is the applied force, $\vec{v}$ is the velocity of the particle and $\vec{B}$ is the magnetic field that the charge is moving through. If a line current is in a magnetic field then each charge making up the current is subject to the same force. A magnetic field perpendicular to the current applies a force which is perpendicular to both the magnetic field vector and the current vector according to the vector cross product (Figure 2).
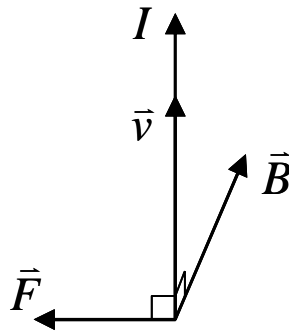
**Figure 2: Force applied due to magnetic field B. B is pointing into the page.**

Consider two parallel steady line currents, $I_1$ and $I_2$. Each current produces a magnetic field which wraps around the current according to the Biot-Savart law. Each current is also in a magnetic field, which yields an applied force (i.e. the magnetic field from $I_1$ induces a force on $I_2$ and vise versa). If the two currents are in the same direction then the applied forces are such that the two currents are attracted towards each other. If the currents are in opposite directions then they repel (Figure 3).
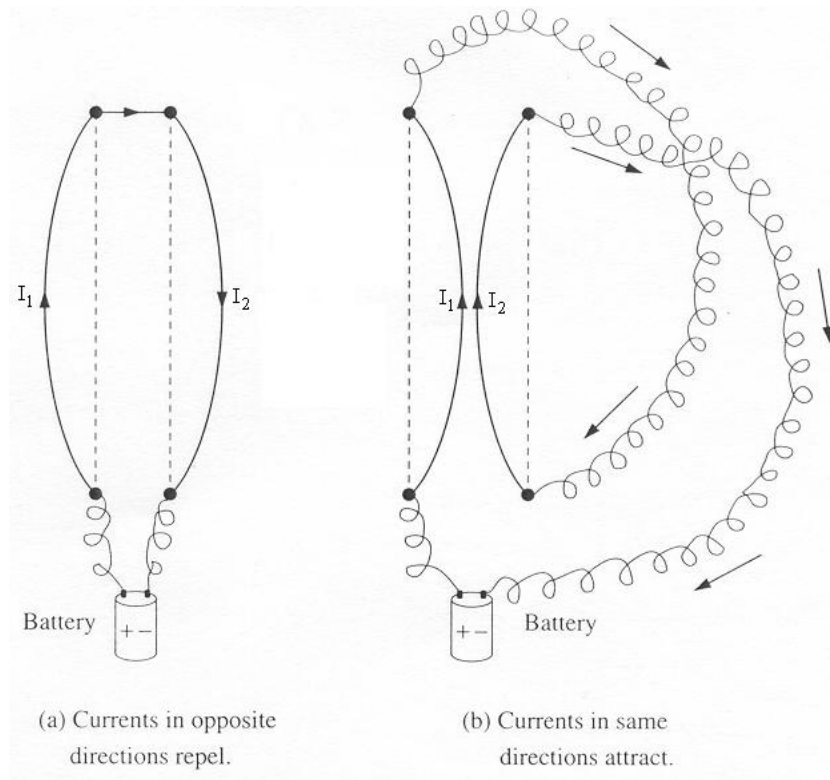
**Figure 3: Forces on parallel currents [2].**
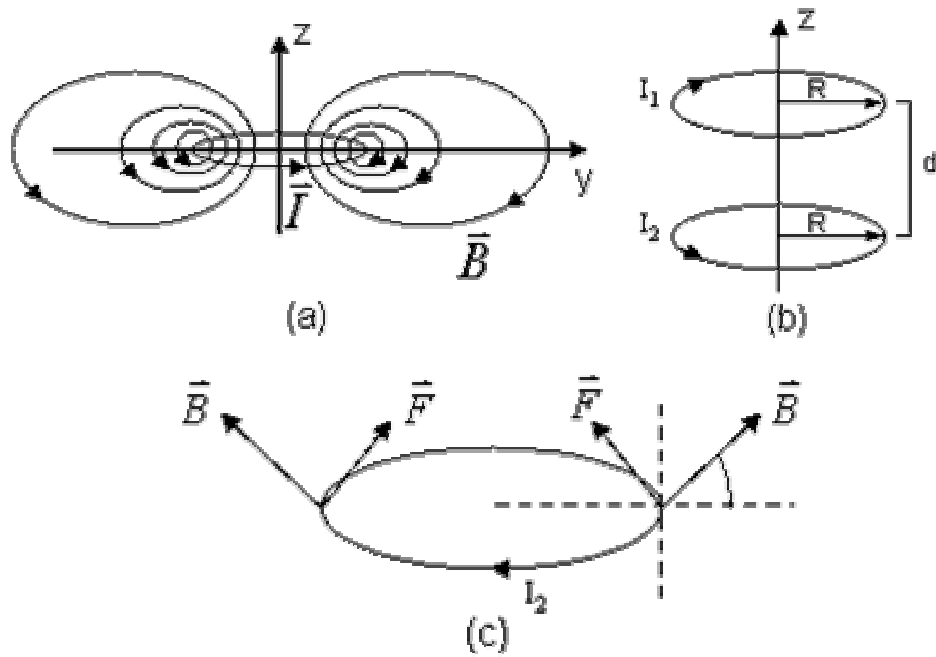


**Figure 4: (a) Magnetic field of a physical dipole (current is going counter clock wise around the z-axis). (b) Stacked current loop configuration. (c) Force applied to upper current loop.**

Magel uses a system of two physical dipoles stacked on top of each other. A physical dipole is a circular loop of current which produces a magnetic field as shown in Figure 4 (a). If two current loops of the same radius are stacked on top of each other with currents going in opposite directions (Figure 4 (b)) then the applied force on the upper loop due to the lower loop is as shown in Figure 4 (c). When d<<R, the net force on the upper ring can be approximated as the force between two parallel line currents of length $2\pi R$, where:

$$\vec{F} = \mu_0 I_1 I_2 \frac{R}{d}.$$

When R<<d, the net force on the upper ring can be approximated as the force between two dipoles, where:

$$\vec{F} = \frac{3\pi\mu_0 I_1 I_2 R^4}{z^4}.$$

Notice that there is a net upward force on the loop. This force is the basis for the first stage of the Magel architecture. Also notice that there is a net stress towards the center of the loop. This stress must be considered when designing Magel.

Consider the case where two current loops are stacked on top of each other, as in Figure 4 (b), and the bottom loop is on the surface of the Earth. There is a gravitational force in the negative z direction pulling the top loop downwards. If the magnetic force on the loop balances out the gravitational force then the resulting system is unstable. If the center of the top loop shifts a small amount away from the z-axis then the net horizontal force on the upper loop is non-zero and there is a net torque.

When the upper loop is off-center, the axial symmetry of the system is broken. The magnitudes and directions of the magnetic fields at the left and right points shown in Figure 4 (c) are different, resulting in different forces at those points. This gives a net lateral force on the upper loop as well as a torque. The net torque on the upper loop ($\vec{N}$) is given by:

$$\vec{N} = \vec{m} \times \vec{B}$$

where

$$\vec{m} \equiv I \int d\vec{a} = I\vec{a}$$
$$\vec{a} = \pi R^2 \hat{z}$$

Here $\vec{m}$ is the magnetic dipole moment and $\vec{a}$ is the vector area of the loop. These are more factors to consider when designing Magel.

Another issue to consider for this system is the case of a changing magnetic field due to the lower ring. Changing magnetic fields induce electric fields. These electric fields induce currents in conducting materials. This includes the conductor containing the current in the upper loop as well as any conductors in electronics, engine parts, second stage, etc. Materials exist that are known to soak up magnetic fields and can be used to protect sensitive components if the induced current is too large. More specifically, the induced electric field ($\vec{E}$) and the electromotive force ($\varepsilon$) can be found by Faraday's law:

$$\varepsilon = \oint \vec{E} \cdot d\vec{l} = -\int \frac{\partial \vec{B}}{\partial t} \cdot d\vec{a} .$$

This shows that, for the stacked loop system, an increasing magnetic field from the bottom loop creates an increase of current in the top loop. The opposite is also true; a decrease in magnetic field from the bottom loop creates a decrease of current in the top loop.

The last topic to consider is superconductivity. There are a number of problems that come about by using conventional conducting materials (copper, iron or gold) to carry the current for the upper ring. These materials have small internal resistance which causes a loss of current and a build up of heat. They are also heavy materials compared to the alternative. SC materials have zero resistance which leads to zero loss of current and no heating. Generally, they are also lighter weight. The tradeoff is more maintenance, elevated cost and higher complexity than conventional conductors. However, they are necessary to maintain the high currents needed for Magel.

Superconductors are materials that have zero electrical resistance and perfect diamagnetism when they are cooled below a certain temperature, called the critical temperature ($T_c$). Perfect diamagnetism means that the material does not allow an external magnetic field to penetrate into its interior. To counteract any applied field, a superconductor will induce its own magnetic field to exactly cancel it. As a result, a superconductor's $T_c$ will lower with an increase in the applied magnetic field, meaning too much magnetic field will cause the SC material to become non-superconducting.

Superconductivity is a broad subject and will not be covered in depth. However, more background is needed and the propulsion analysis will cover the missing details.

## Design Methodology

The design methodology used focuses on designing a launch system which is comparable to the D4H. The D4H was chosen because it currently has the largest payload capability of all modern expendables. To more closely compare the two systems, the second stage of Magel was based off of the second stage of the D4H.

Figure 5 shows the design structure matrix (DSM) used to design Magel. This stems from a standard launch vehicle DSM. There is a large convergence loop between the configuration and weights and sizing analyses. There is also a loop between operations and both cost and safety. The feedback link from weights and sizing to configuration is rather weak, so the configuration does not change often and the main convergence loop is between propulsion and weights and sizing.
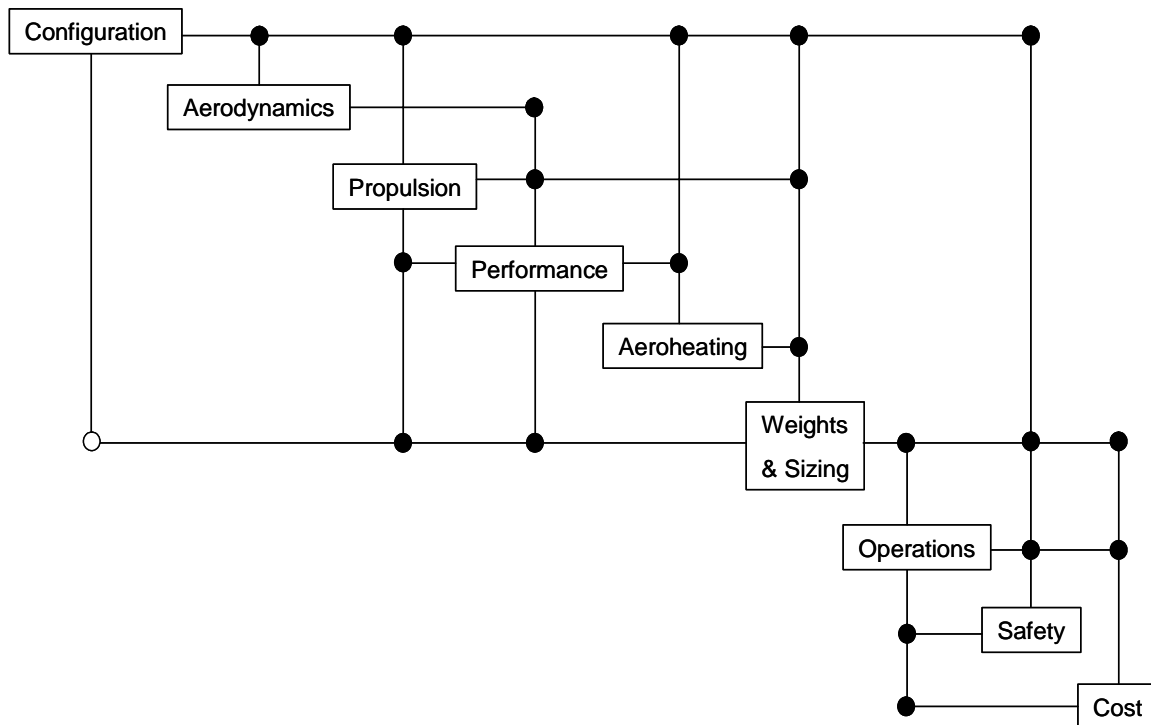


**Figure 5: DSM used for Magel.**

## Mission Scenario

The Magel architecture replaces the first stage of an expendable rocket with a reusable vehicle. The first stage of the system consists of a large (6.6 km diameter) ring that houses seven SC tubes. These tubes carry enough current to propel the ring into the atmosphere by pushing against the magnetic field provided by another current ring on the surface. The second stage of the system is an expendable rocket. During the ring's ascent, the second stage is towed behind the first stage, connected to the ring by cables.

At launch, the first stage and the attached second stage rest on top of the ground ring (Figure 6). When the two rings (one composes the first stage, the other is the ground station) have been charged up to their initial current, the first stage is released. The first stage ascends upwards, towing the second, until the upward force on the ring vanishes. At this stage the vehicle is going 726 m/s vertically (Mach 2.44) and the ring is at 20 km altitude. At that time the second stage is released from the cables and is ignited. This single stage rocket then ascends into a 100 nmi by 100 nmi 28.5° orbit. Shortly after the second stage is released (while the cables still have some horizontal motion towards the outside of the ring), the cables detach from the first stage, fall into the ocean and are later recovered. When the first stage starts to fall back down to Earth, it uses the magnetic force applied by the ground ring to slow its descent and make a soft landing back onto the ground ring. During the whole trajectory, the current of the ground site is controlled to yield the optimal performance.

## Disciplinary Analyses

Conceptual design of the vehicle used several disciplinary analyses to analyze the feasibility and viability of the system. They are presented here in order of execution within the DSM.

**2nd stage ascends to orbit**

**2nd stage is released and cables fall to Earth**

**1st stage launches towing 2nd stage**

**1st stage descends and lands back on ground site**

**Magel starts on top of ground site**
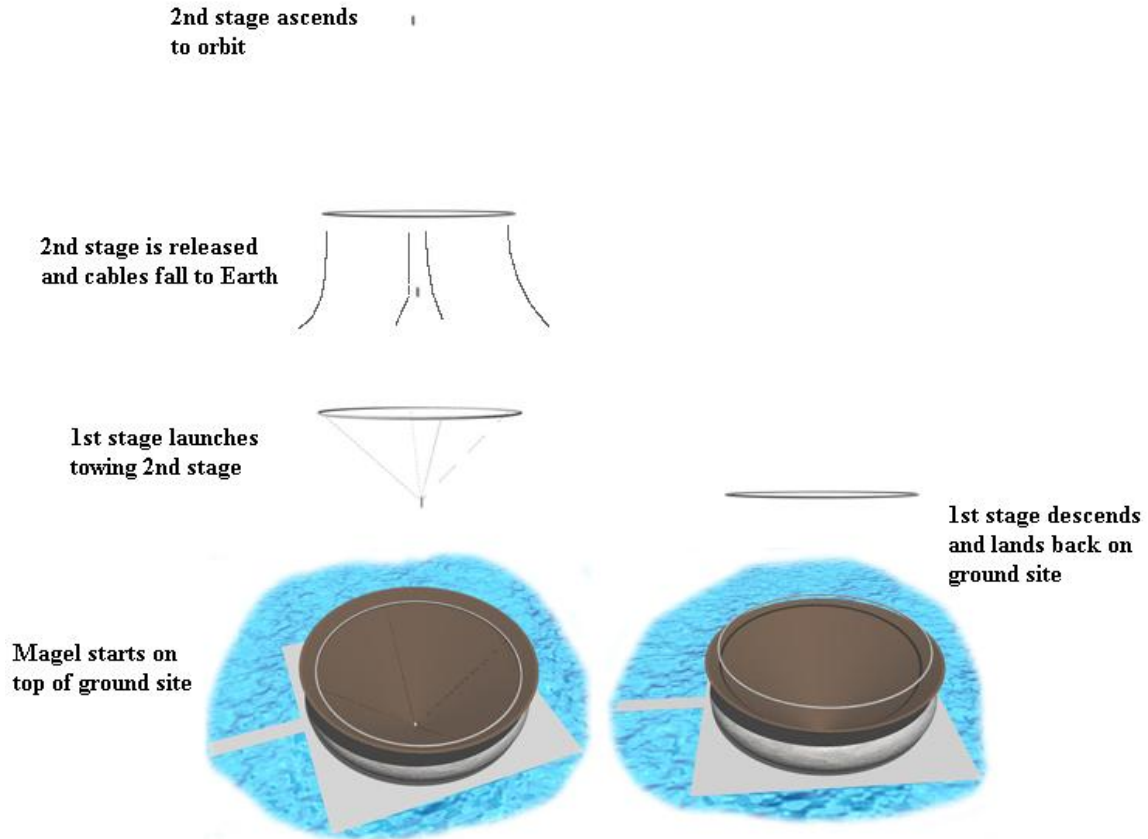
**Figure 6: Magel mission profile.**

## *Configuration*

Configuration of the vehicle was determined using Pro/ENGINEER (Pro/E). Size estimates for each of the subsystems on the vehicle where obtained from the weights and sizing analysis. These values were used to draw a computer aided design (CAD) model of the system. This model was then used to determine available space and, more importantly, to provide a model for the aerodynamics analysis.

The baseline vehicle configuration is shown in Figure 7 and Figure 8. The second stage rocket is positioned on the axial line of the vehicle and is suspended from the first stage by four cables. These cables are angled at 45° with respect to the horizontal. The first stage ring is 6.6 km in diameter and the second stage hangs 3.3km below the ring.

A closer view of the first stage shows more interesting details (Figure 9). The

cross section of the ring is an airfoil shape with a height to width ratio of 2.5 (5.4m by 2.2m) (Figure 8). This allows enough volume to house seven SC tubes, the attitude determination and control system (ADCS) engines and all of the ADCS propellant. There are four ADCS engines and propellant tanks positioned around the ring, one for each ADCS engine.
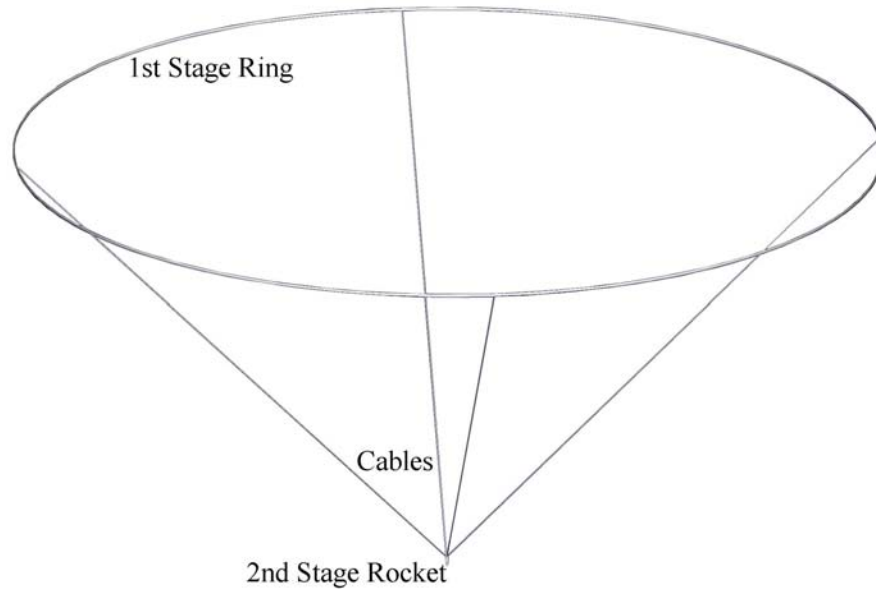


**Figure 7: CAD model of Magel (isometric view).**
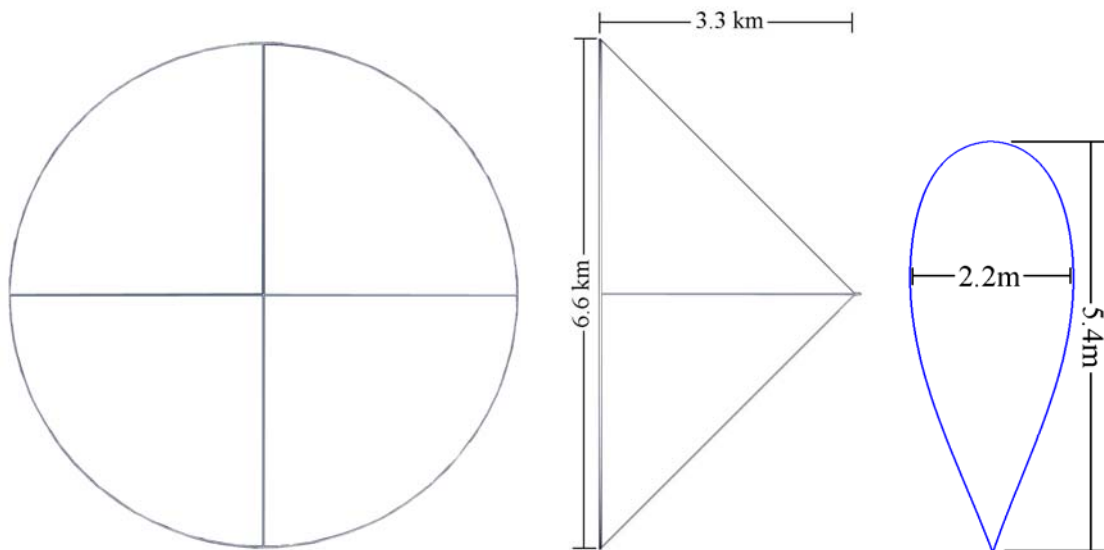


**Figure 8: Top view (left), side view (middle) of Magel. Cross section of first stage ring fairing (right).**
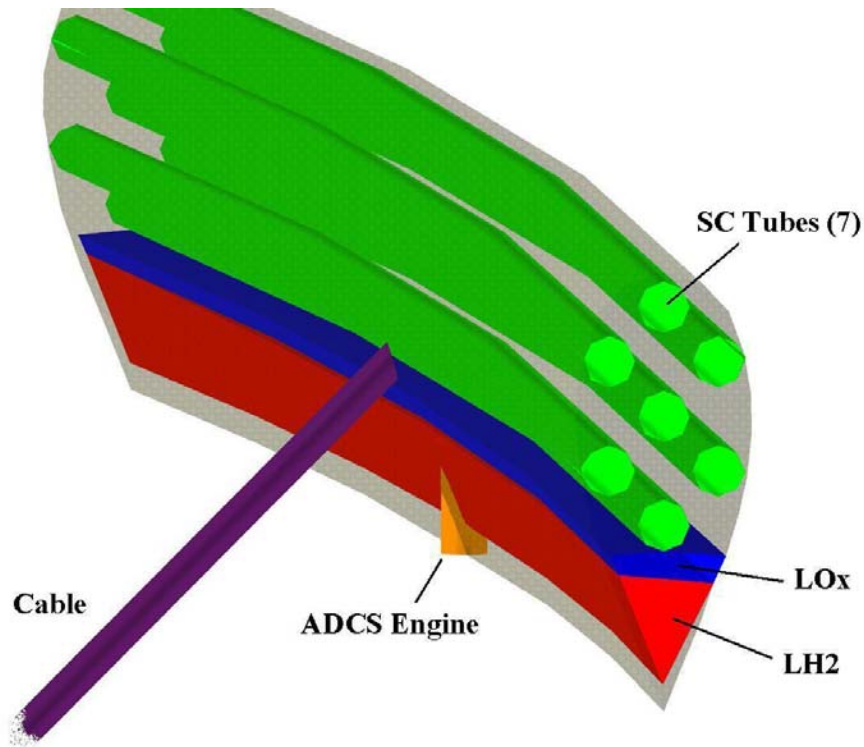
**Figure 9: First stage breakdown, zoomed in.**

## *Aerodynamics*

Aerodynamics analysis was performed with Configuration Based Aerodynamics (CBAero) version 1.4.1. CBAero is a preliminary aerodynamics tool for predicting subsonic to hypersonic aerodynamic environments about an arbitrary vehicle configuration [3]. For subsonic aerodynamics, CBAero uses an unstructured, fast multi-pole panel formulation and for the supersonic and hypersonic regimes it uses a variety of independent panel type methods. This software is currently being developed by David J. Kinney at NASA Ames Research Center. The parts of the software that are still in development were not used in this analysis.

In order to feed the model into CBAero, a mesh was made from the CAD model. Pro/Mesh, a meshing tool in the Pro/E family, would normally be used for this task, but that package was not available. Instead, the CAD model was converted into IGES format and imported into IDEAS. The meshing tool in IDEAS was then used to make a triangular mapped mesh of the ring and the second stage. The meshes were exported as ANSYS files and imported into CBAero.

For the first stage trajectory, only the aerodynamics of the ring was considered.

The components from the cables, second stage and engines were considered negligible. For this configuration, there were no base triangles and only one wake edge, the edge formed by the trailing edge of the ring's airfoil shape. The reference area used was the "wing" area of the airfoil (circumference x height = 17,700 m$^2$) and the reference chord used was the diameter of the ring (6.6 km). Analysis was done over the entire regime provided by the trajectory. Mach number (M) ranged from 0 to 3, dynamic pressure (q) ranged from 0 to 0.422 atm and angle of attack ($\alpha$) was from 0 to 10°. The trajectory itself did not sway from an $\alpha$ other than 0°, but other $\alpha$'s were considered for completion.

The second stage analysis was also performed to find drag coefficients and for completion. The base triangles for this configuration included the area below the nozzle and the area on the bottom face of the engine. Wake edges included the nozzle edge and the bottom edge of the engine. The horizontal cross section of the rocket (20.3 m$^2$) was used as the reference area and the diameter (5.08 m) was the reference chord. Analysis was done over the entire regime provided by the trajectory: M from 0 to 20, q from 0 to 0.422 atm and $\alpha$ from 0 to 50°.

CBAero's visualization tool was used to display the pressure profiles for the two analyses (Figure 10 and Figure 11). The profiles are displayed at the maximum pressure condition in the first stage trajectory (maximum q and the maximum M attained at that q). These figures show that the maximum pressure on the ring is at the top of the airfoil (the leading edge) and is symmetric about the centerline of the vehicle. The maximum pressure on the second stage is near the nose and is symmetric about the centerline. These results are reasonable and help to prove the validity of the analysis.

CBAero also provides lift and drag coefficients over the specified regime. For the first stage, charts of $C_{dt}$ vs M, $C_{lt}$ vs $C_{dt}$ and $C_{lt}/C_{dt}$ vs $\alpha$ for various M's are shown in Figure 12. The drag profile was used in the performance analysis. It gave a peak $C_{dt}$ of 0.76 at M=1.54. The other two charts show results that are not reasonable for standard vehicles. This may be due to the fact that the vehicle has such low lift. These results were not used in any other analysis but they suggest that CBAero's results may not be valid. Nonetheless, the drag profile can be considered a good estimate of the drag and was therefore used.
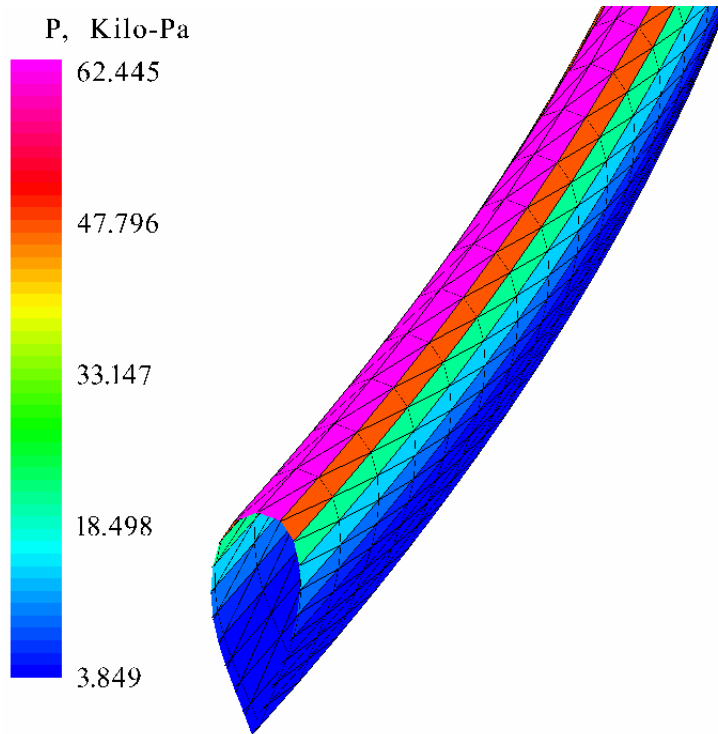
Mach: 2.186, Atmospheres: 0.422, Alpha: 0.000

**Figure 10: Pressure profile of the ring at the maximum condition.**
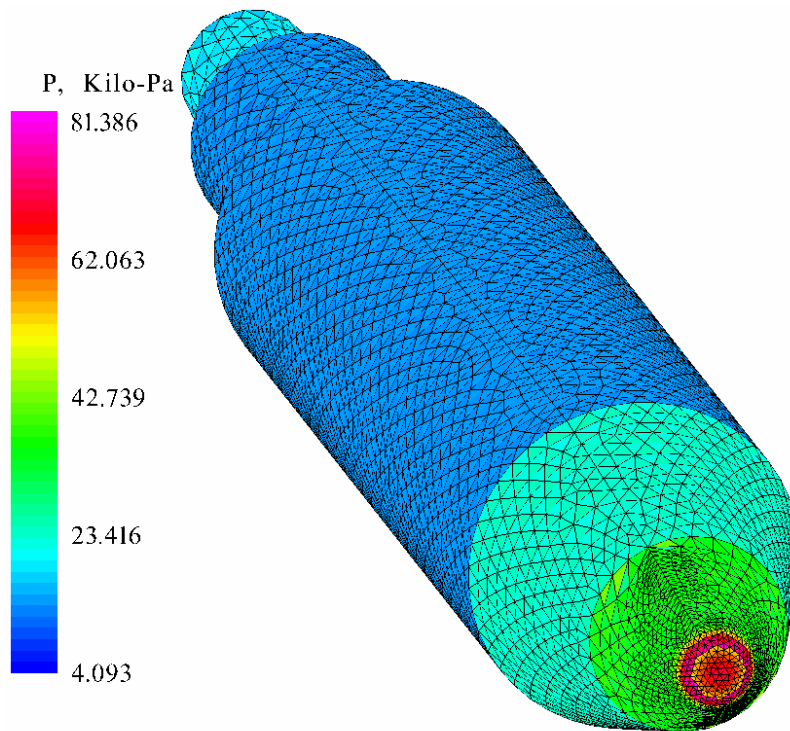


Mach: 2.120, Atmospheres: 0.422, Alpha: 0.000

**Figure 11: Pressure profile of the second stage at the maximum condition.**
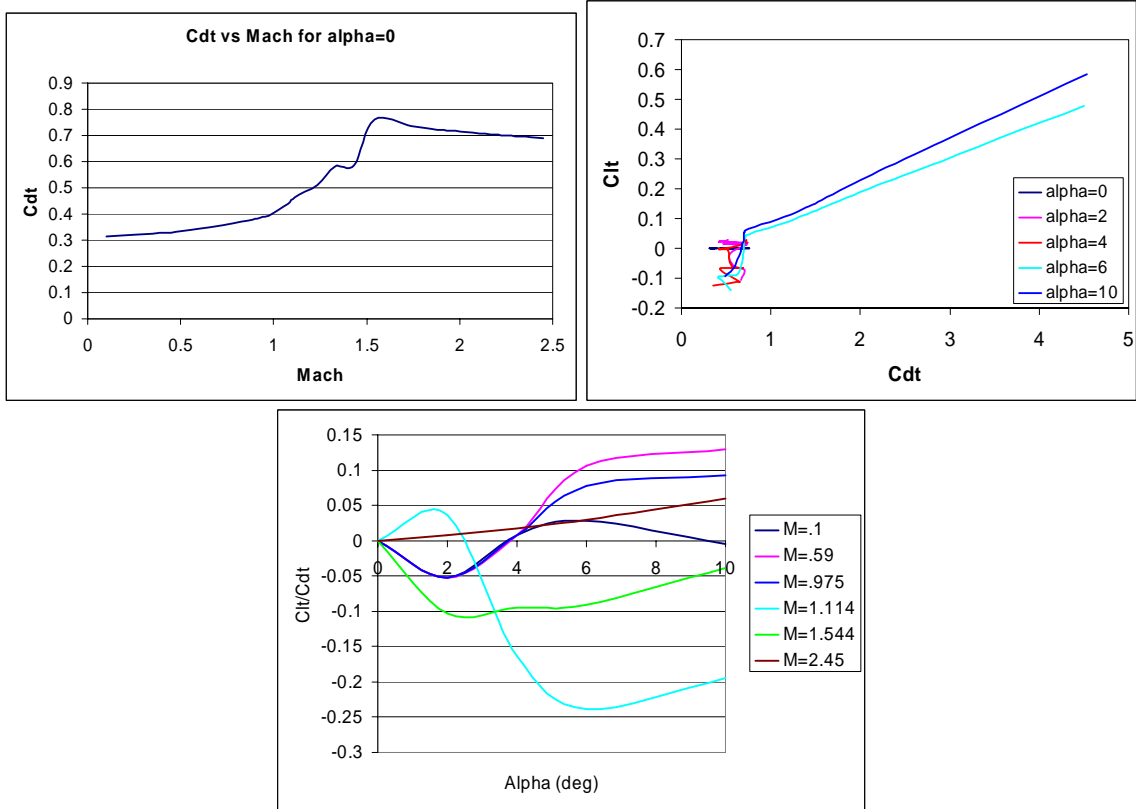
**Figure 12: $C_{dt}$ vs Mach for $\alpha=0$ (top left). $C_{lt}$ vs $C_{dt}$ for several $\alpha$'s (top right). $C_{lt}/C_{dt}$ vs $\alpha$ for several M's (bottom).**

## *Propulsion*

The design of the individual SC tubes was taken from StarTram (Figure 13) [4]. One tube consists of a structural support tube, an outer heat dispersing tube, the superconducting material and a flow of liquid helium. This design allows for good structural support and cooling of the SC material.

The main structure for each tube consists of a graphite epoxy honeycomb composite support tube. This supports the tube from collapsing in on itself due to the radially inwards magnetic pressure ($P_m$) caused by the tube's own magnetic field, where:

$$P_m = \frac{(B_{max})^2}{2\mu_0}.$$

Here, $B_{max}$ is the maximum magnetic field in the SC material induced by its own current. This is the magnetic field at the outer surface of the tube. Tubes were designed to withstand 5 times their rated pressure in the worst case scenario to ensure an adequate

14

safety margin.

Wrapped around the tube are the strands of SC wires. These are wrapped in a helix around the tube for the full circumference of the ring. The NbTi SC strands are mixed with Cu with a Cu/NbTi ratio of 1.3/1, similar to those proposed for the Superconducting Super Collider [4].

## A. Longitudinal Cross Section

Superconductor Winding

Overlapping Sliding Joint On Aluminum Support Tube

A

Aluminium Support Tube

Overlapping Sliding Joint On Honey-Comb Composite Support Tube

Liquid Helium

Honey-Comb Composite Support Tube

A

Superconductor Winding

## B. Superconductor Winding Pattern (Not To Scale)

Helical Winding Of Separate Conductors

Conductors Not Shown

Conductors Not Shown

**Figure 13: Longitudinal cross section of a SC tube (A) and SC winding pattern (B) [4].**

A high purity (99.999%) aluminum tube is used to ensure excellent heat conduction [4]. This tube is on the outer surface of the structural tube, under the SC wires. It is used to disperse random heat fluctuations that may occur in the SC wires and pull heat away from the SC wires towards the liquid helium (LHe) cooling fluid.

LHe flows through the support tube to cool the SC wires. NbTi has a $T_c$ of 9.3 K [8], so the cooling fluid used must cool the SC wires to a temperature that is lower than this. LHe is the best alternative in terms of cost, weight, boiling point and the fact that it is a noble gas. This will cool the wires to LHe's boiling point at 4.2 K.

The entire SC tube system was designed to have high safety margins and good structural support. Seven tubes carry the total current needed for the first stage (1.2e7 A). In the worst case scenario, two entire SC tubes are allowed to transition to their normal state and cease to carry current. If that happens, the current being carried by these tubes is transferred over to the other five tubes.

The seven SC tubes are configured into a tightly packed geometry (Figure 14). This design provides good packaging efficiency inside the airfoil as well as structural support. Truss segments are positioned between several sets of SC tubes to support the structure and provide a counter force to the attractive force between each tube. Truss segments are made out of graphite epoxy with an operating compression strength of 7.5e8 N/m$^2$. The force between each tube was approximated as the force between two line currents. The truss must also provide support against the laterally inward force due to the ground magnetic field, which is at its maximum at the maximum altitude, as well as counter act the force coming from the tension in the cables connecting the second stage. Each truss segment was sized to withstand five times a compressive force equal to the maximum force between each SC tube plus the sum of the lateral ground force and the cable forces averaged by the number of SC tubes to ensure a good safety margin. The truss is represented by the thick lines shown in Figure 14.

The propulsion analysis used electrodynamics to size the current carrying system based on values from weights and sizing. Given $M_{gross}$ and the maximum altitude, and assuming that the maximum magnetic moment of the ground site is 200 times the moment of the first stage ring, it was possible to find the current needed in the first stage and maximum current of the ground site in order to cancel the gravitational force at the

maximum altitude (20 km).

The size of each SC tube relied on the SC material properties. The minimum cross sectional area of SC material needed for each tube ($A_{min}$) was determined from the critical current density ($J_c$, the maximum allowable current per cross sectional area) of NbTi, such that:

$$A_{min} = I_{max} / J_c$$

where $I_{max}$ is the maximum current applied to any single tube. With the critical magnetic field ($B_c$, the maximum allowable magnetic field in the SC material) of NbTi, it was then possible to find the minimum radius of each SC tube ($R_{min}$) using:

$$R_{min} = \frac{\mu_0 I_{max}}{2\pi B_c}.$$

The optimized value of this radius is actually much larger than this lower limit. For the baseline, $A_{min} = 0.00422$ m$^2$ and $R_{min} = 0.15$ m.

$B_c$, $J_c$ and $T_c$ are all related. $B_c$ goes up with a decrease in T (Figure 15). To a good approximation:

$$B_c(T) = B_c(0)\left[1 - \left(\frac{T}{T_c}\right)^2\right].$$

Also, $J_c$ increases with $B_c$ such that:

$$J_c = B_c / \mu_0 \lambda$$

where $\lambda$ is the penetration depth of the magnetic field. For Magel, T is fixed at 4.2 K (boiling point of LHe) which yields a $B_c$ of 11.9 T. As an added safety margin, the maximum operating $B_c$ used was 9.5 T (80% of original). The $J_c$ for this system was 5e9 A/m$^2$ [4], but the maximum operating $J_c$ used was 2.8e9 A/m$^2$ (56% of original).
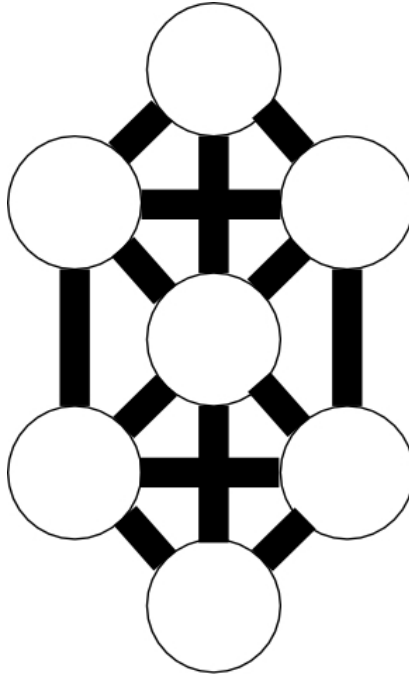
**Figure 14: Truss and SC tube geometry.**
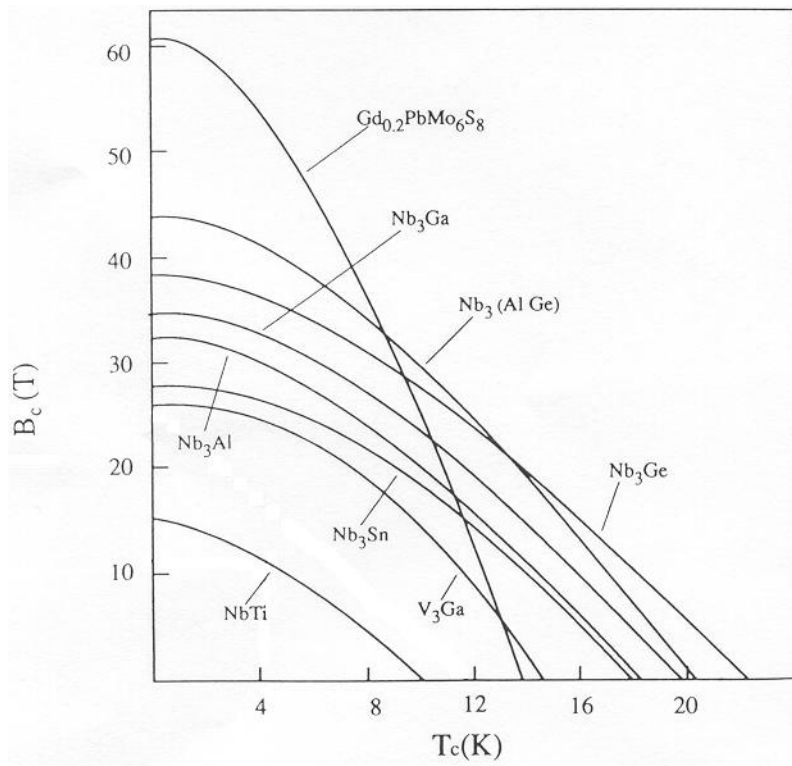


**Figure 15: Relationship between critical magnetic field and critical temperature for the best classical superconductors [8].**

Analysis of the ADCS system was based on a rough estimate of the amount of propellant needed to correct a small change in the trajectory. Assuming the ADCS makes a trajectory correction to reposition the entire first stage so that it's directly over the center of the ground ring every time the first stage is off by 2 m, it takes 6 m/s of velocity change to reposition the vehicle and that a correction of this magnitude occurs 100 times over the entire first stage trajectory, the total delta V needed by the ADCS was 600 m/s. The thrust needed from each ADCS engine was sized to 150% of the thrust needed to counteract the maximum torque applied by the ground ring's magnetic field, which was 6.5e5 N.

Each ADCS engine is a sized Space Shuttle Main Engine (SSME). The amount of propellant needed for the ADCS was considerable (1.7e6 kg). In order to save mass, an efficient SSME was chosen over a pressure fed system which would add weight due to the pressurized gas needed. This assumes the technology that an SSME-type engine can be created such that it can start and stop quickly and repeatedly.

The second stage propulsion analysis is a simple model based on a modified rocket equation. The rocket was sized based on the total delta V needed to get to orbit. The delta V needed to make the flight with no losses is $V_{final} - V_{initial}$. The delta V loss from drag was estimated to be 0 m/s because the rocket starts its ascent where the atmosphere is very thin (0.15 kg/m$^3$ and 9.2 K-Pa). The delta V losses from gravity and thrust vector control (TVC) were based on the losses due to these factors from an average expendable over an entire flight (~686 m/s for each [5]). They were scaled linearly by the distance from the initial second stage altitude (16.7 km, staging point) to the altitude of payload fairing separation (132 km for D4H [6]). The altitude of payload fairing separation was used because at this point the rocket is nearly horizontal and practically in orbit about Earth. There was also a delta V gain due to the Earth's rotation because this is a prograde launch. A summary of these values is listed in Table 1.

Other masses were sized from existing components. Inert mass and payload fairing mass were taken from the D4H [6]. Engine mass and $I_{sp}$ were sized from an SSME based on the thrust required (120% of the total weight).

**Table 1: Delta V losses for the second stage.**

| Type | Delta V Loss (m/s) |
|---|---|
| Flight | 7,068 |
| Drag | 0 |
| Gravity | 599 |
| TVC | 599 |
| Rotating Earth | -396 |
| | |
| **Total** | **7,870** |

## *Performance*

Performance calculations used a simple altitude step method to compute the trajectory of the first stage. Values for the initial altitude, maximum acceleration ($a_{max}$=6 g's, including gravity, based on D4H payload requirements), maximum q ($q_{max}$=42.6 KPa, based on D4H payload fairing), gross mass ($M_{gross}$=1.10e7 kg) and the drag profile were provided. The maximum current of the ground station ($I_{g,max}$, where $I_g$ is the current of the ground station) is the current needed to balance the gravitation force of the gross mass at an altitude of 20 km. Small steps in altitude (30 to 250 m) were taken until the maximum altitude was reached. At each step the trajectory conditions were calculated based on the previous step. The atmospheric model used simple equations from Glenn Research Center [7].

A final first stage altitude of 20 km was chosen to restrict the capabilities of the architecture. This ensures that the first stage does not escape from Earth and it provides a limit on the size of the vehicle. Also, it provides a staging point for the second stage that has little atmospheric density. It is possible to launch the first stage ring into orbit, greatly reducing the second stage mass, but this option was rejected because of the problems with getting the ring back down to Earth without damage. The cost for the first stage ring is very large, so loosing the vehicle is out of the question.

Each phase of the trajectory is limited by $a_{max}$, $q_{max}$ or $I_{g,max}$. Initially the trajectory is limited by $a_{max}$, at the end of this phase q will rise to $q_{max}$. During the next phase, the vehicle accelerates slowly, keeping $q=q_{max}$, until $I_g$ rises to $I_{g,max}$. The vehicle will then rise until a=0, at which point the second stage will ignite. There is also a point in the trajectory where the magnetic force from the ground station switches from using

the calculation based on two circular line currents to the calculation based on two dipoles. At this point the current needed by a line current ($I_{g,line}$) is equal to a current needed by a dipole ($I_{g,dipole}$). This trajectory is the most efficient way to reach the maximum altitude with the given constraints (in terms of maximum final velocity). The conditions between each phase in the trajectory are listed in Table 2.

**Table 2: Conditions at key points in the first stage trajectory.**

| State | Time (s) | Alt (m) | Vel (m/s) | M | q (Pa) |
|---|---|---|---|---|---|
| Initial Condition, $a=a_{max}$, $q<q_{max}$ | 0.0 | 24 | 0 | 0.00 | 0 |
| $q=q_{max}$, $a<a_{max}$ | 5.5 | 778 | 272 | 0.81 | 42,109 |
| $I_{g,line}=I_{g,dipole}$, $q=q_{max}$, $a<a_{max}$ | 10.5 | 2,175 | 292 | 0.88 | 42,109 |
| $I_g=I_{g,max}$, $q<q_{max}$, $a<a_{max}$ | 40.8 | 14,431 | 628 | 2.11 | 42,109 |
| 2nd Stage Ignition, $q<q_{max}$, $a=0$ | 48.8 | 20,000 | 726 | 2.44 | 23,453 |

The equations used to calculate the magnetic force are based on the force between two circular line currents and between two dipoles, as discussed earlier. The actual equations used are the same as those discussed, but with an added geometric effects coefficient. The original equations are multiplied by this constant to create a more conservative calculation. For this geometry, the value used for this constant was 0.9 [4]. The imperfection was used because these equations are only approximations. There are geometric effects from the physical dipoles that make the exact expressions for the force equations very complex.

The conditions throughout the first stage trajectory are shown in Figure 16. There are abrupt changes in the charts due to transitions between each phase of the trajectory, as expected. The largest concern here is the discontinuity in the magnetic field at the first stage due to the ground site at the end of the first phase. This is due to the large change in acceleration at this point. To control this change, the current in the ground facility must quickly change from a value of 1.03e7 A to 2.65e6 A in less than one second. Realistically, changes in current at this rate are not feasible with current technology. One alternative would be to gradually change the current over this point. The analysis assumed that the ground site has complete control over the current in the ground ring to simplify the trajectory.

The maximum rate of change in magnetic field at the first stage was small (~6.1e-4 T/s, not including the discontinuity). This is a small rate (the Earth's magnetic field is

4.5e-5 T at the surface), although their still may be some problems with induced electric currents in subsystems.  The amount of material needed to protect sensitive components was assumed to be negligible when compared to the mass of the first stage.  The amount of current that is gained from this change in magnetic field (it is a gain because the magnetic field is increasing and points in the direction opposite of the first stage magnetic moment) was also assumed to be negligible.
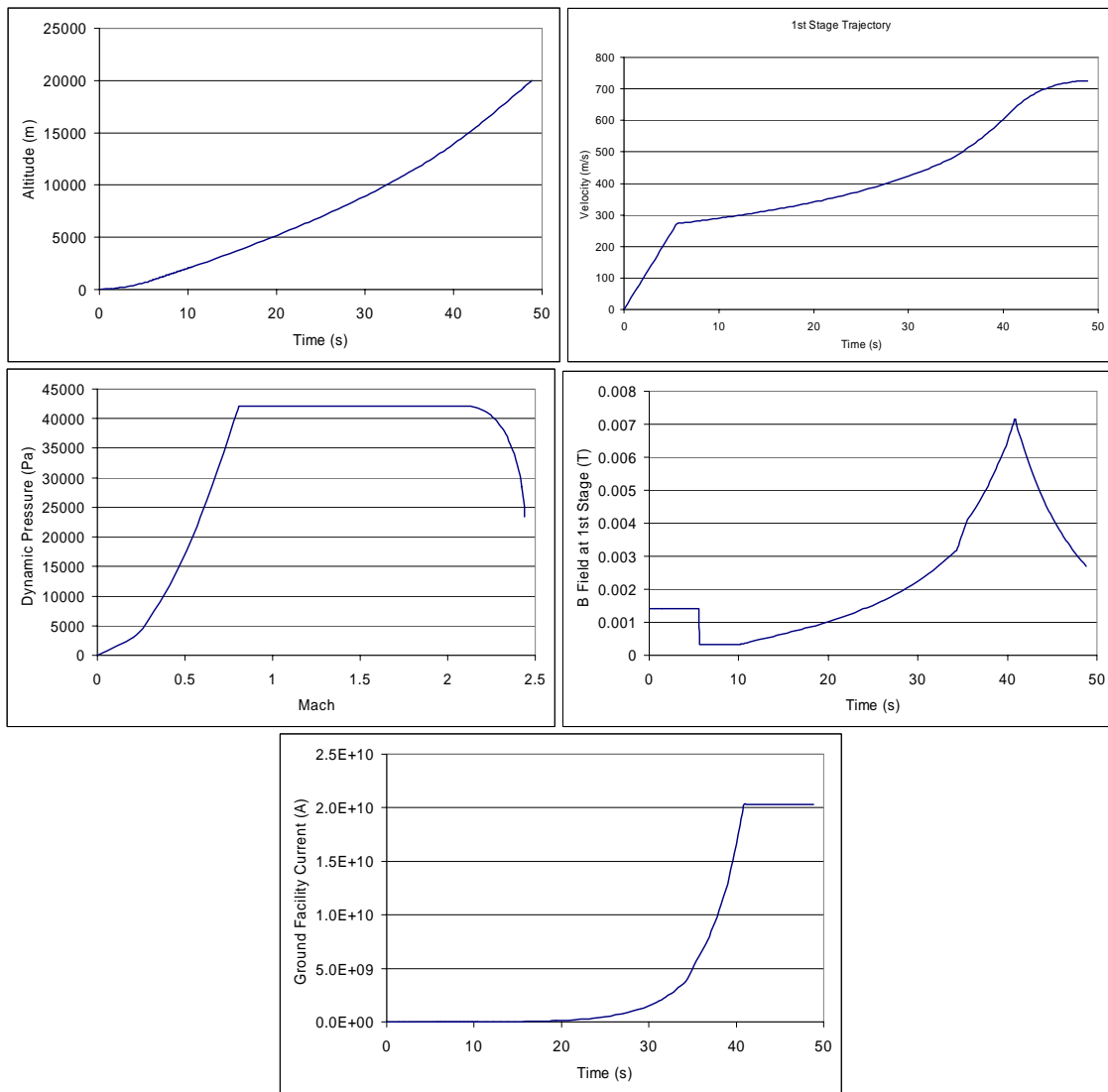


**Figure 16: Conditions for the first stage trajectory.**

## *Aeroheating and Thermal*

Miniver was used for the aeroheating analysis. This code predicts aeroheating boundary conditions for a given cross section, trajectory and ambient conditions. It was developed by NASA Langley Research Center in the early 90's. Analysis was only done for the first stage ring because the contribution of thermal protection system (TPS) mass due to any other part of the vehicle is negligible compared to the mass of the ring.

Inputs to Miniver include several points to define the cross section, a trimmed trajectory and conditions along the specified trajectory. The cross section was defined by providing the running length and cone half angle at several points along the outer edge of the cross section. Ten points were used for this analysis, spaced out evenly along the vertical axis from the top of the cross section to the maximum width. A nose radius of 2.2 m was also given for the first point. The trimmed trajectory used fifty points spaced evenly in time throughout the first stage trajectory. Values for time, altitude, velocity, $\alpha$ and $\beta$ (yaw angle) were given.

Results from Miniver consisted of peak temperature values for each of the 10 points provided. These values were then combined with the CAD model to form Figure 17. The peak temperature attained was 451.8 K at the top of the cross section. A conservative estimate for the melting point of aluminum (the material on the skin of the ring) is 533 K. Therefore, there is no need for any TPS on the ring skin.

TPS for the rest of Magel was neglected. Realistically, there may be an impinging sock wave on the cables that tow the second stage. There may even be a shock cone that intersects with the second stage. Heating effects due to these cases were assumed to be small enough such that the problem could be solved by added TPS to the effected areas. The weight of this TPS was assumed to be much smaller than that of the entire vehicle, and thus was neglected.
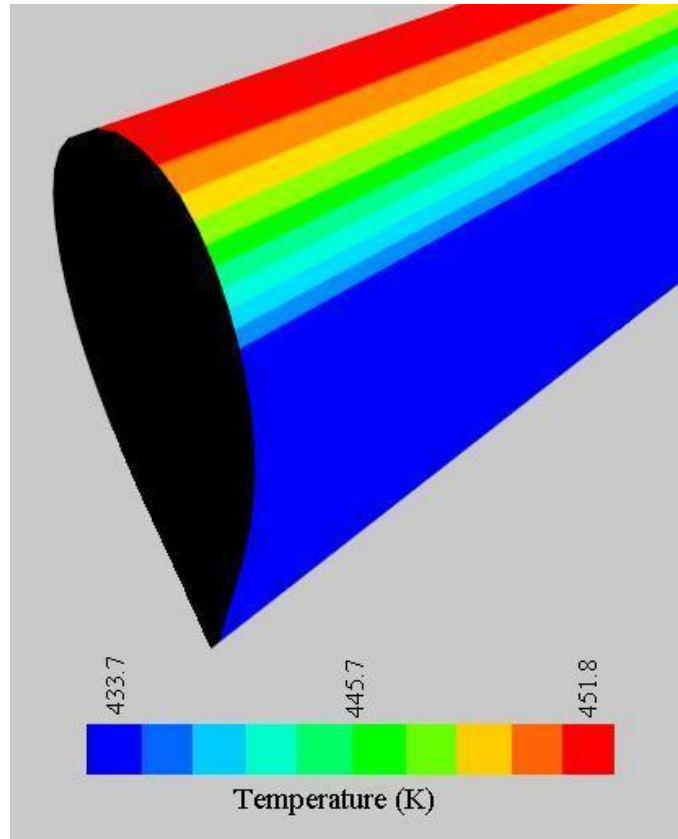
**Figure 17: Peak temperature profile for the first stage ring.**

## *Weights and Sizing*

Magel was sized based on existing components, estimations from StarTram and reusable launch vehicle (RLV) mass estimating relationships (MERs). This analysis was spreadsheet based, using inputs from the configuration, propulsion, performance and aeroheating analyses. It produced values for subsystems masses, total mass and vehicle dimensions (Table 3, Table 4, Figure 18).

**Table 3: Scale of Magel baseline.**

| Component | Value |
|---|---|
| Diameter First Stage (m) | 6,556 |
| Airfoil Width (m) | 2.2 |
| Airfoil Height (m) | 5.4 |
| Total Airfoil Volume (m$^3$) | 160,000 |
| Diameter SC Tube (m) | 0.83 |
| Cable Length (m) | 4,636 |

**Table 4: Weight breakdown for Magel baseline.**

| Component | Mass (kg) | Weight (lbs) |
|---|---|---|
| Ring Fairing | 3.35e6 | 7.40e6 |
| SC Tubes | 1.48e6 | 3.25e6 |
| SC Truss | 3.22e5 | 7.10e5 |
| SC Cooling | 1.28e6 | 2.81e6 |
| ADCS | 1.70e6 | 3.75e6 |
| Cables | 3.18e5 | 7.02e5 |
| Dry Margin | 1.01e6 | 2.23e6 |
| Payload | 2.58e4 | 5.69e4 |
| 2nd Stage | 1.89e5 | 4.17e5 |
| | | |
| **Total Dry** | **6.75e6** | **1.49e7** |
| **Gross** | **1.10e7** | **2.41e7** |
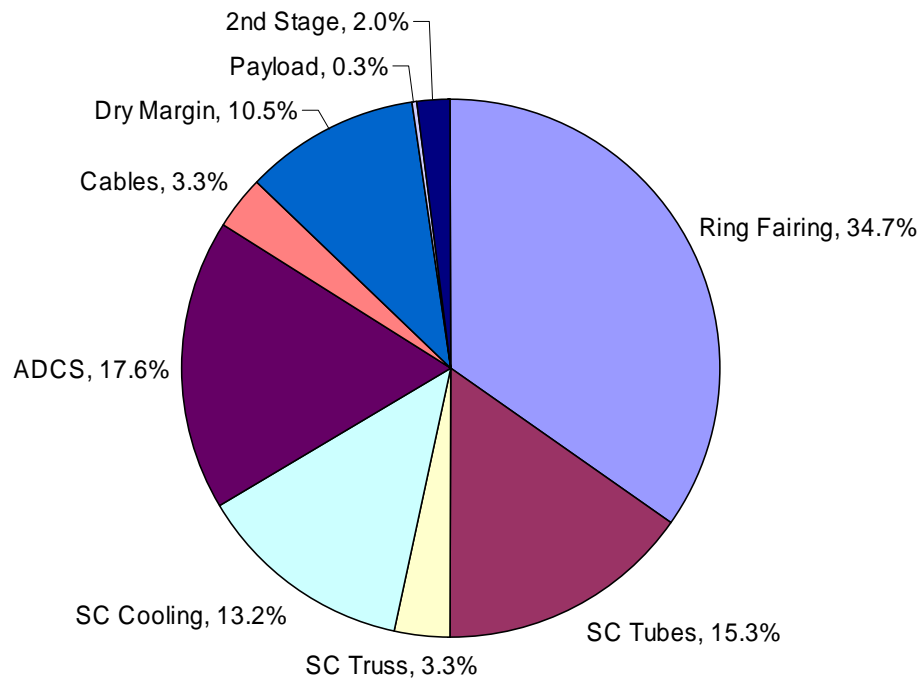


**Figure 18: Weight breakdown for Magel baseline.**

There were four main components for the first stage body: the ring fairing, ring truss, SC material and SC tubes. The amount of SC material needed was sized from the $J_c$ and the radius of the first stage ring. The SC tubes were sized from the ring radius and the amount of magnetic pressure imposed. Mass for the ring fairing used an MER for RLV wing fairing weight [9], where:

$$M_{ring-fairing} = S_{fairing} \left( 0.0002499 q_{max} + 1.7008 + \left( 0.00003695 q_{max} - 0.003252 \right) b_{body} \right).$$

Here $S_{fairing}$ is the surface area of the fairing (267,000 m$^2$) and $b_{body}$ is the maximum width of the ring cross section (2.16 m). Each strut composing the truss was sized based on the maximum axial force it needs to support (as discussed earlier). The maximum force per unit length between the shorter members of the truss was 1.20e6 N/m and was 8.47e5 N/m for the longer members. Struts were made from graphite epoxy with an operating compression strength of 7.5e8 N/m$^2$ [4].

The cooling system mass was sized from the SC tube size. This system consists solely of the LHe flowing inside each of the SC tubes. Mass of the LHe assumed that there was at most a 15 cm thick flow on the inside of each tube (i.e. the flow of LHe was shaped like a hollow cylinder with a 15 cm wall thickness) [4]. Masses for other parts of the cooling system were assumed to be negligible compared to the total mass of LHe needed.

Cables connecting the second stage were made from oriented polyethylene and were sized based on the maximum tension in each cable. Each cable runs from the first stage ring down to the second stage at a 45° angle. The maximum vertical tension in all of the cables is equal to the force needed to pull the weight of the second stage and the weight of the cables themselves at the maximum acceleration. A 400% safety margin on the operational tensile strength (6e8 N/m$^2$ [4]) was used.
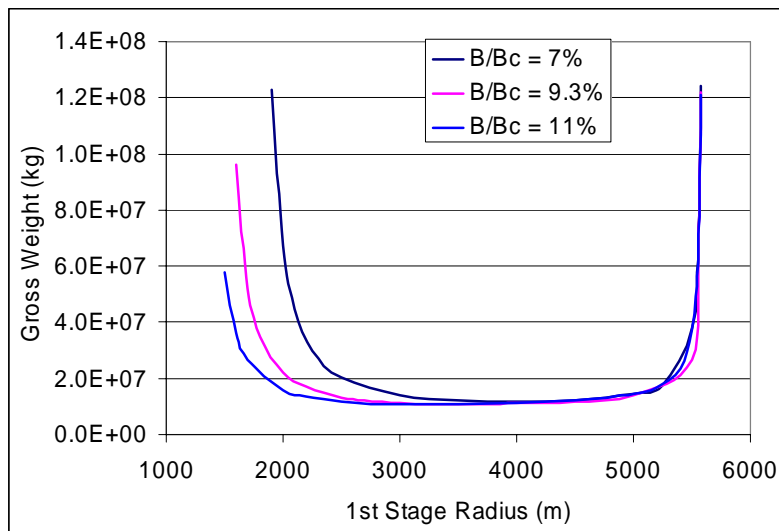


**Figure 19: 1$^{st}$ stage ring radius study for various B$_c$ percentages.**

Other contributions to mass were also considered. Mass of the ADCS system as well as the second stage gross mass were inputs from the propulsion analysis. Also, a dry mass margin of 15% was included.

The radius of the first stage ring as well as the radius of each SC tube were independent variables for the mass analysis. The vehicle can be closed within a range of values for these radii. Outside these ranges, the mass of the vehicle blows up. Figure 19 shows how the gross mass changes with ring radius and SC tube radius. $B/B_c$ is the value of the magnetic field at the outer surface of each SC tube as a fraction of $B_c$, which indirectly controls the SC tube radius. For each $B/B_c$ considered, the mass of the vehicle is finite when the first stage ring radius is between ~2 km and ~ 5.5 km. For the baseline design, ring radius and SC tube radius were optimized such that the life cycle cost (LCC) of the vehicle was minimized with the loss of vehicle failure rate constrained to be less than 1 in 4000 flights.

## *Operations*

The operations analysis used Architecture Assessment Tool-enhanced (AATe), originally developed by NASA KSC. AATe is a spreadsheet based program that allows for quick estimations for fixed and variable operations costs as well as the vehicle turn around time (TAT) and available flight rate. Inputs include vehicle masses and sizes, vehicle design life, loss of vehicle reliability and total design, development, testing and evaluation (DDT&E) and theoretical first unit (TFU) costs. Magel is most likely outside the range of AATe's domain of validity, but it is a good approximation for the design.

Magel's operation settings were specified for AATe. The analysis assumed that Magel was a highly automated system and used a dedicated turnaround and assembly facility. It also assumed that Magel is a reusable system with some expendable components.

AATe made some propulsion assumptions. It assumed that the propulsion system is partially integrated (main propulsion is separate from ADCS but these are vastly different systems). There are seven main engines with no moving parts and this is a two stage vehicle. Also, the Magel concept requires no use of toxic or polluting materials.

27

Operations assumptions deal with vehicle reliability and complexity. Magel uses only custom minimum weight components. It is completely fault tolerance to support flight safety, but accepts loss of mission. Only a few active components are needed for flight with no more than three systems that require monitoring. The system is extremely complex because it has multiple stages and requires a very large ground facility. Lastly, Magel is a multistage vehicle which permits component replacement requiring no personnel to enter the vehicle.

Various assumptions for fluid uses are also needed by AATe. Magel uses no toxic fluids in any flight or ground systems that restrict ground operations. It is a multi-stage system that only requires two fluids stored in two tanks (not including the LHe). Also, Magel requires no on-board stored gases.

There are also a few other systems that AATe considers. Magel requires a ground power system with a power production infrastructure. All systems have non-intrusive and non-mechanically active sensors. Magel provides adequate environmental control during flight without using heat shields, but requires ground support before launch. Finally, there is a large amount of payload flexibility.

Baseline operations outputs from AATe are given in Table 5. Fixed operations cost is largely due to the size of the vehicle. Therefore, a large value for the fixed operations cost was reasonable compared to the overall size of Magel. The facilities cost was much smaller than expected due to the fact that AATe does not take into account launch assist systems. This cost was increased in the vehicle cost analysis to more accurately account for the complex ground system. Finally, AATe does not take into account that fact that the second stage was expendable. The cost of the second stage was added to the variable operations cost in the cost analysis.

**Table 5: Baseline operations metrics from AATe. All dollar amounts are given in FY 2003.**

| Variable | Value |
|---|---|
| TAT (Days) | 14.3 |
| Available Flight Rate (Flights/Year) | 25.5 |
| Fixed Operations (M$/Year) | 27,300 |
| Variable Operations (M$/Flight) | 9.70 |
| Facilities (M$/Site) | 3,010 |
| Variable Labor (M$/Flight) | 7.30 |
| Variable Line Replacement Unit (M$/Flight) | 2.39 |
| Fixed Labor cost (M$/Year) | 104 |
| Fixed Line Replacement Unit (M$/Year) | 30.8 |

## *Safety and Reliability*

Safety and Reliability analysis used GT-Safety II v1.6. This is a spreadsheet based code that works by multiplying various failure rates together. Values from the configuration, operations and weights and sizing were used to obtain the vehicle's reliability. Separate analyses were done for each stage of the vehicle.

For the first stage, all of the safety adjustment factors in GT-Safety were set to best describe the first stage of Magel. Magel was assumed to be four times safer than Space Shuttle in terms of abort options/windows, internal vehicle health monitoring (IVHM), flight system redundancy, safety margins and ground handling complexity. It was assumed to be mildly safer than Space Shuttle in terms of landing mode, use of toxic and volatile fluids, propellant loading process and staging, flying, launching and landing over a population. Landing area flexibility was assumed to be ten times less safe than Space Shuttle because Magel can only land directly on the ground site. The single engine shutdown rate was sized with the ring radius (seven SC rings were considered to be the first stage main engines). Propellant type versus TNT equivalent was sized with the total ADCS propellant. Lastly, vehicle subsystem failure rates were set to 10% of those for an average expendable.

For the second stage, the safety adjustment factors were set to describe a future expendable. The second stage was assumed to be ten times safer than Space Shuttle in terms of IVHM, ground handling complexity, use of toxic and volatile fluids, the propellant loading process, and staging and flying over a population. It was also assumed to be mildly safer than Space Shuttle in terms of safety factors. The single

engine shutdown rate was assumed to be the average for a rocket engine at 1 in 6,000. As for the first stage, the values for the vehicle subsystem failure rates were set to 10% of those for an average expendable.

According to GT-Safety, the baseline vehicle was very safe with these assumptions. The loss of mission reliability was 1 in 2,248 mean flights between failure (MFBF) and the loss of vehicle was 1 in 5,076 MFBF. This is roughly twelve times the reliability of Space Shuttle. Note that a loss of the second stage vehicle was considered as a loss of mission for the whole vehicle. The baseline economic scenario gives the safety outputs in Table 6.

One safety concern that was not handled by GT-Safety is the effect of the magnetic field of the ground current on the environment. Humans can withstand being in a magnetic field of 1.5 mT [10] or in a changing magnetic field of 0.03 T/s [11] without harm. The minimum lateral distance away from the ground site where these conditions are satisfied is 17.5 km. Therefore, if the ground site is to be placed near KSC, it must be at least 17.5 km out in the ocean.

**Table 6: Safety summary. Assumes 20 flights per year.**

| Reliability | Value |
|---|---|
| Loss of Mission MFBF | 1 in 2,248 Flights |
| Loss of Mission MTBF | 1 in 112.4 Years |
| Loss of Vehicle MFBF | 1 in 5,076 Flights |
| Loss of Vehicle MTBF | 1 in 253.8 Years |
| Casualty Rate | 0.0192 Deaths/Year |
| Total Time Between Casualties | 1 in 52.0 Years |

## Cost and Economics

Cost estimation of Magel used the NASA-Air Force Cost Model (NAFCOM). This uses a historical database to estimate cost based on subsystem weights. Airframe and propulsion costs are estimated separately. NAFCOM was used to estimate the DDT&E and TFU cost for both the Magel vehicle and ground site (Table 7).

For the vehicle estimation, component weights for each subsystem on each stage were input. Next, complexity factors for each cost component were determined. The first stage was said to be built in segments that are 16 m long (the length of a railroad

car).  Each of these segments are very similar; only difference being the four segments with ADCS engine and cable connections, the eight segments with end caps on the ADCS propellant tanks and some segments have ADCS propellant tanks in them and some do not.  Therefore, all segments were estimated to be the same cost and have the same learning curve.  The TFUs for the first stage and the ground ring were assumed to have a learning curve rate of 85% such that the cost per segment as a function of the segment number is:

$$C_{segment}(n) = (1-R)e^{-.1n} + R$$

where $C_{segment}$ is the fractional cost of segment number n as a percentage of the first segment cost and R is the learning curve rate.  This means that if enough segments are built, the cost of each segment will eventually reach 85% of the cost of the first segment.  Also, the complexity factors for integration, assembly and checkout for both the airframe and the first stage propulsion were linearly scaled from the total number of segments needed.

A similar approach was used for the ground site cost estimation.  The ground ring was considered to be much less complex than the launch vehicle because it is only composed of SC rings and it does not have to be flight ready.  This assumption lowered complexity factors across the board and is responsible for its relatively low cost compared to its weight.  The total facilities cost per site was the sum of the costs to build the ground ring structure, given by NAFCOM, and the cost to build the facility infrastructure (roads, platform, buildings, etc.), given by AATe.

Table 7: Cost estimates from NAFCOM for Magel baseline.

| Variable | Cost (B$ FY 2003) |
|---|---|
| Launch Vehicle DDT&E | 52.7 |
| Launch Vehicle TFU | 29.8 |
| Ground Site DDT&E | 59.4 |
| Ground Site TFU | 45.0 |

At first, the Cost and Business Analysis Module program was used to estimate the economic scenario.  Various values were taken from the weights and sizing and operations analyses to create the module.  Unfortunately the economic scenario would

not close; no value for the price per pound could produce a net present value of 0$ at the end of life of the vehicle. This was due to the fact that as the price per pound to orbit increased, the market capture percentage decreased. The price per pound was so high that Magel did not capture any of the available market even with a 100% market expansion rate. To solve this problem, a much simpler approach was used.

The final economic analysis used was a spreadsheet based tool created solely for Magel. It simply sums all of the costs of the vehicle to find the LCC assuming values for the engine life (500 flights), vehicle life (1000 flights), program length (30 years) and flight rate (20 flights/year). It also includes a 15% cost margin and assumes that the market does not change over the life of the vehicle (0% market expansion rate), there is no profit and there is zero cost of money. This implies that the cost of the vehicle (TFU and DDT&E) is paid for upfront. Economic results for the baseline vehicle are given in Table 8.

Notice that the baseline cost per pound to orbit is $35,500 FY 2003/lbs. When compared to the D4H price per pound of $3,000 FY 2003/lbs [6], Magel's cost is unacceptable. One way to reduce this cost is to change the program length or flight rate. This is not a bad choice because these variables were assumptions.

Trade studies were performed on this design to examine the effects of program length and flight rate on the cost per pound to orbit (Figure 20). For every program length considered, cost per pound to orbit decreased more than exponentially with flight rate. This is because the fixed cost is rather large compared to the variable cost. Meaning, the higher the flight rate the more the fixed cost gets distributed into the cost of each flight. The minimum flight rate needed to compete with the D4H (to get the cost per pound down to $3000 FY 2003/lbs) decreases with an increase in program length, however, there is a tradeoff in total flights needed (Table 9).

**Table 8: Economic results for Magel baseline. All dollar amounts are in FY 2003.**

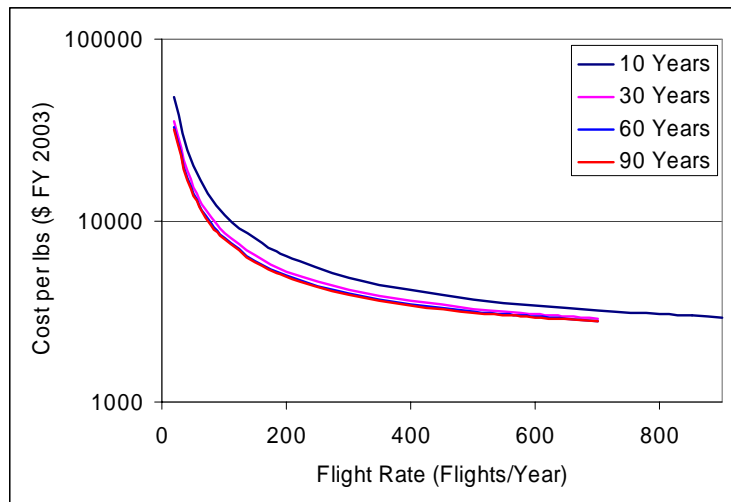| Variable | Cost |
|---|---|
| DDT&E (Launch Vehicle and Facilities) (B$) | 112 |
| TFU (Launch Vehicle Only) (B$) | 29.7 |
| Facilities Cost (Includes Facilities Ops. Cost) (B$/Site) | 48.0 |
| Fixed Cost (B$/Year) | 27.5 |
| Variable Cost (Includes $2^{nd}$ Stage Cost) (M$/Flight) | 64.4 |
| Cost Margin (15%) (B$) | 182 |
| | |
| **LCC (B$)** | **1,210** |
| **Cost per Pound to Orbit ($/lbs)** | **35,500** |



**Figure 20: Flight rate trade study for various program lengths.**

**Table 9: Minimum flight rate needed to compete with the D4H for various program lengths.**

| Program Length (Years) | Minimum Flight Rate (Flights/Year) | Total Flights |
|---|---|---|
| 10 | 852 | 8520 |
| 30 | 626 | 18780 |
| 60 | 576 | 34560 |
| 90 | 559 | 50310 |

## Baseline Conclusions

The Magel baseline yields a cost per pound to orbit that is not competitive with current expendables. The D4H costs a conservative $3000/lbs to a 100 nmi by 100 nmi orbit [6]. With the baseline economic assumptions (20 flights/year for a program length of 30 years) Magel's cost is roughly twelve times that; not an outrageous amount, but enough not be competitive. However, these cost results involve some economic uncertainty. In order to get a better estimate of Magel's viability, a Monte Carlo simulation (MCS) was done, which will be explained later.

There are still several problems with the Magel architecture. There are impinging shockwaves on the cables as well as a possible impinging Mach cone on the second stage. The two stacked current ring geometry is unstable, which leads to the large ADCS system mass. Corrections due to high winds or the Coriolis Effect were not considered and may also make large contributions to the ADCS. Structural modes in the first stage ring and cables may prove to make the airframe unstable. There are induced currents in anything conductive on the vehicle due to the changing magnetic field of the ground ring. Not to mention the problems from the shear size of the vehicle.

Finally, there were several issues with the tools used for this design. NAFCOM, AATe and GT-Safety were created for normal RLVs, like Space Shuttle. Most likely, Magel is outside the acceptable limits of these tools. Therefore, other, more general tools are needed for better estimations. Still, these tools provide rough estimates for the vehicle and are a good first step.

## ROSETTA Model

After the baseline vehicle was designed, a Reduced-Order Simulation for Evaluating Technologies and Transportation Architectures (ROSETTA) model was built. This is a spreadsheet based tool that fully integrates all components of the design into a simple tool to quickly estimate the effects of small changes in variables. It is necessary, when running a large number of cases for the input variables, to considerably reduce the computation time for each point in the design space.

Creating the ROSETTA model was fairly straightforward. Most of the contributing analyses were already spreadsheet based. For these analyses, it was a

simple matter of just integrating them into one spreadsheet. Aerodynamic results, like drag coefficients, changed very little when the scale of the vehicle changed. Therefore, the ROSETTA model used the baseline aerodynamics results for all cases. Aeroheating was mostly affected by the trajectory used (the shape of the airfoil was constant), which changes very little throughout the design space because it is mostly determined by $a_{max}$ and $q_{max}$, which are constants. Therefore, the baseline aeroheating results were used for all designs.

On the other hand, the operations analysis was not so simple to integrate. Indeed it was a spreadsheet based analysis, but it was unable to be imported into the ROSETTA model due to a bug in Microsoft Excel. Instead, a response surface equation (RSE) was created to take its place. Using Phoenix Integration's ModelCenter v5.0.1 and Spaceworks Engineering's ProbWorks RSE v1.1 generator, RSE's for each of AATe's outputs were created using a second order central composite design of experiments on the following variables: loss of vehicle reliability, vehicle design life, insertion weight, vehicle length and width (height is always 2.5 time the width), DDT&E and TFU. $R^2$ values for each of these RSEs were all nearly 1.

## Economic Monte Carlo Simulation

The baseline cost results contain various economic uncertainties. In order to get a better estimate of Magel's viability, an MCS was done. This analysis involved using Crystal Ball in combination with the ROSETTA model to vary all of the uncertain economic variables and obtain probabilistic results for the economic metrics. Crystal Ball is a Microsoft Excel macro that facilitates the simulation. Economic variables are considered to be noise variables (the designer has no control over them) so triangular probability density functions were used over their ranges. These variables as well as their ranges are listed in Table 10.

After running the MCS with 5000 iterations, cumulative distribution functions (CDFs) were created for each of the economic metrics (Figure 21). Values for these metrics at the 50% confidence mark were considered to be the final results (Table 11). This gives a cost per pound to orbit of $38,900 FY 2003/lbs; which is roughly thirteen times that of a D4H. With these economic assumptions, the baseline Magel architecture

is most likely not viable (especially since the 0% confidence of cost per pound is six times more than the D4H).

**Table 10: Economic variables and their ranges used for the economic MCS.**

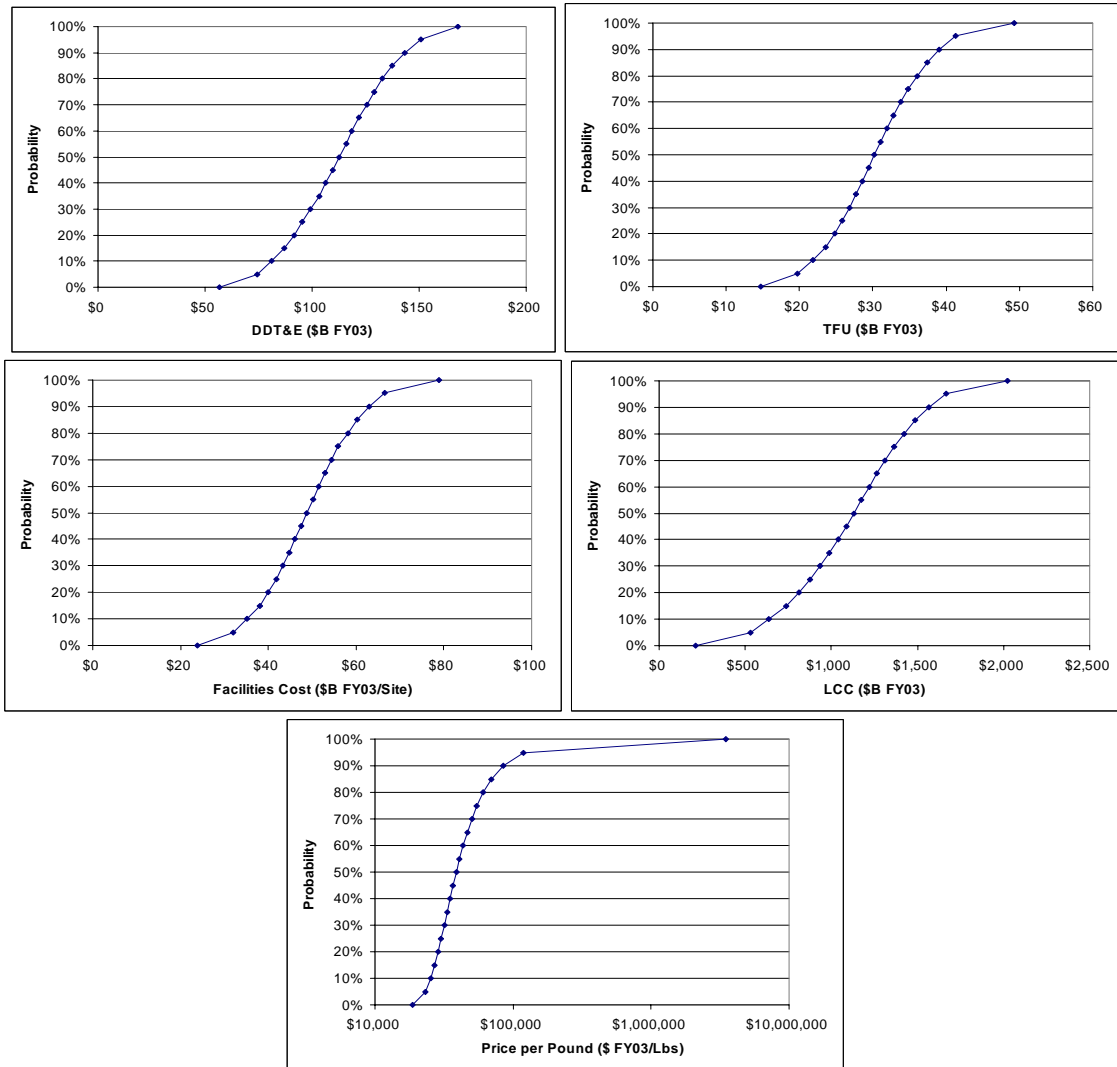| Variable | Minimum | Nominal | Maximum |
|---|---|---|---|
| Engine Life (Flights) | 100 | 500 | 1,000 |
| Vehicle Life (Flights) | 100 | 1,000 | 2,000 |
| Program Length (Years) | 1 | 30 | 50 |
| Learning Curve Rate | 0.75 | 0.85 | 1 |
| Flight Rate (Flights/Year) | 0 | 20 | 40 |
| TFU Complexity Factor | 0.5 | 1 | 1.5 |
| DDTE Complexity Factor | 0.5 | 1 | 1.5 |



**Figure 21: CDFs for economic MCS.**

**Table 11: Economic metrics at 50% confidence. All dollar amounts are in FY 2003.**

| Metric | Value at 50% Confidence |
|---|---|
| Total DDT&E (B$) | 113 |
| TFU (B$) | 30.2 |
| Facilities Cost (B$/Site) | 48.8 |
| LCC (B$) | 1,130 |
| Cost per Pound to Orbit ($/lbs) | 38,900 |

# Technology Infusion

To help improve the feasibility and viability of Magel, several technologies were considered. Since the SC tube system is the main driver for the design, the main focus of the technology infusion was on different types of SC materials. These technologies were infused into the baseline design; the resulting designs were compared to the baseline.

## *Technology Identification*

Three different types of SC materials were considered as well as technology impacts on magnetic field geometry and subsystem masses. SC materials considered include NbTi, Nb$_3$Sn and (Bi,Pb)$_2$Sr$_2$Ca$_2$Cu$_3$O$_x$ (BSCCO). For other technologies, general improvement in the geometric imperfection coefficient, ADCS mass, airfoil fairing mass, SC truss mass and SC support tube mass were considered.

NbTi is the most common SC material currently in use and was used as the baseline. Typical values for density, J$_c$ and B$_c$ are 6,530 kg/m$^3$ [12], 5e9 A/m$^2$ [4] and 12.2 T [8] respectively. Large quantities are used in the competitive MRI magnet business and have brought the cost down considerably. The current estimate is around $1 FY2001/k-Am [13].

Nb$_3$Sn is another common SC material currently in use. Typical values for density and B$_c$ are 8,036 kg/m$^3$ [12] and 19.0 T [8]. A promising value for J$_c$ of 6e9 A/m$^2$ has also been reported [14]. Currently, only small quantities of Nb$_3$Sn are being produced (2.5 tons/year) for an expensive $4.6 FY 2001/k-Am [13]. If the demand for this material reaches 250 tons/year, this price could be brought down to $1.5 FY 2001/k-Am [13]. Magel would create this demand, therefore, the lesser cost was assumed.

The leading high temperature superconductor is BSCCO. Currently, BSCCO is

only available in powder form. Tubes of the material have been demonstrated to have peak values for $J_c$ of 2e9 A/m$^2$, but only locally [15]. Typical values for density and $B_c$ are 4,010 kg/m$^3$ [12] and 465.5 T [8, 15]. The current cost of BSCCO is $1,000 FY2001/k-Am [16]. With decreases in costs and new manufacturing techniques, the cost of BSCCO is predicted to decrease considerably to $21 FY 2001/k-Am [16]. This smaller cost was assumed for the following analyses.

Improvements in other subsystems are not related to specific technologies, but represent general improvements that can be expected. The baseline design was considered to be a worst case scenario, so all of ranges for these technologies were set to lower the vehicle's mass. Mass improvements in the airfoil fairing, SC truss and SC support tubes were based on improvements in materials. For the ADCS mass, once technology improvement could be to include all of the ADCS functionality in the ground ring (i.e. changing the magnetic field from the ground ring to control the first stage) or have some other ground based ADCS system. Therefore, a lower bound of 0 on the ADCS mass could be expected. Finally, improvements for the geometric effects coefficient were based on different ground ring geometries that could be considered (i.e. having the ground ring in the form of a solenoid or using an iron core in the center of the ring).

## *Technology Monte Carlo Simulation*

In order to evaluate the effects of infusing each technology, several MCSs were performed. The effects of infusing each of the SC materials were well understood. Instead of including each of these materials in a single MCS, three separate MCSs were run (one for each SC material). For example, one MCS consisted of infusing Nb$_3$Sn and running the MCS over the other five technologies. Technology impact factors used for the SC materials and the ranges used for the other technologies are listed in Table 12 and Table 13.

Values for the SC materials were derived from the values previous stated. Distributions on these impacts were not included because the effects of the technologies were known relatively well and the model takes a considerable amount of time to optimize the ring radius and SC tube radius each time the SC material properties are

changed. The effects of the SC material technologies cause relatively large changes in the optimum ring radius and SC tube radius and therefore the model would have to be optimized for every iteration of the MCS to obtain good results, which would take a considerable amount of time for a 5000 iteration MCS.

The ranges for the other technologies were based on general improvements that could be expected. For these technologies the optimum ring radius and SC tube radius did not change very much with a change in impact factor. Therefore, the design did not have to be optimized for every MCS iteration to obtain good results.

After infusing each of the SC materials, the radius of the first stage ring and the radius of each SC tube was again optimized to minimize LCC. Gross mass for $Nb_3Sn$ was 1.10e7 kg and for BSCCO was 1.23e7 kg; weight breakdowns are shown in Figure 22 and Figure 23. Diameter of the first stage ring was 6596 m and 7614 m and the diameter of each SC tube was 0.83 m and 0.84 m for $Nb_3Sn$ and BSCCO respectively. Cost per pound to orbit for $Nb_3Sn$ was \$35,700 FY 2003/lbs and was \$41,300 FY 2003/lbs for BSCCO. Both of these technologies showed an increase in gross mass and cost compared to the baseline (NbTi).

Table 12: Technology impacts for SC material.

| Variable | NbTi | Nb3Sn | BSCCO |
|---|---|---|---|
| Density SC Material | 1 | 1.23 | 0.614 |
| Jc | 1 | 1.20 | 0.4 |
| Bc | 1 | 1.56 | 38.1 |
| Cost SC Material | 1 | 1.5 | 21 |

Table 13: Ranges for general technology impacts considered.

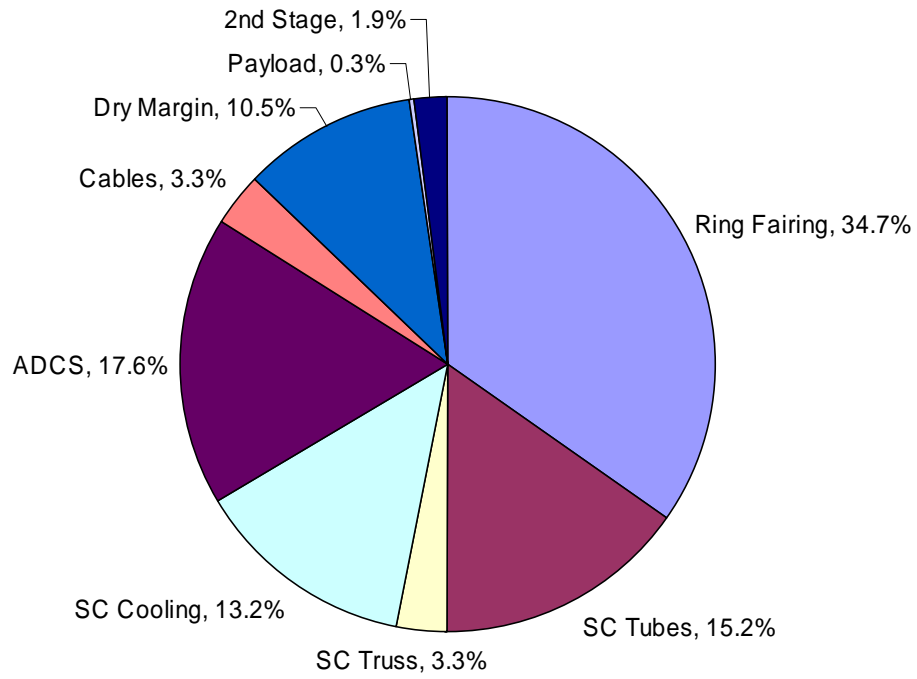| Technologies | Minimum | Nominal | Maximum |
|---|---|---|---|
| Geometric Imperfection Factor | 1 | 1 | 1.1 |
| Mass ADCS | 0 | 0.5 | 1 |
| Mass Airfoil Fairing | 0.8 | 0.9 | 1 |
| Mass SC Truss | 0.8 | 0.9 | 1 |
| Mass SC Support Tube | 0.8 | 0.9 | 1 |

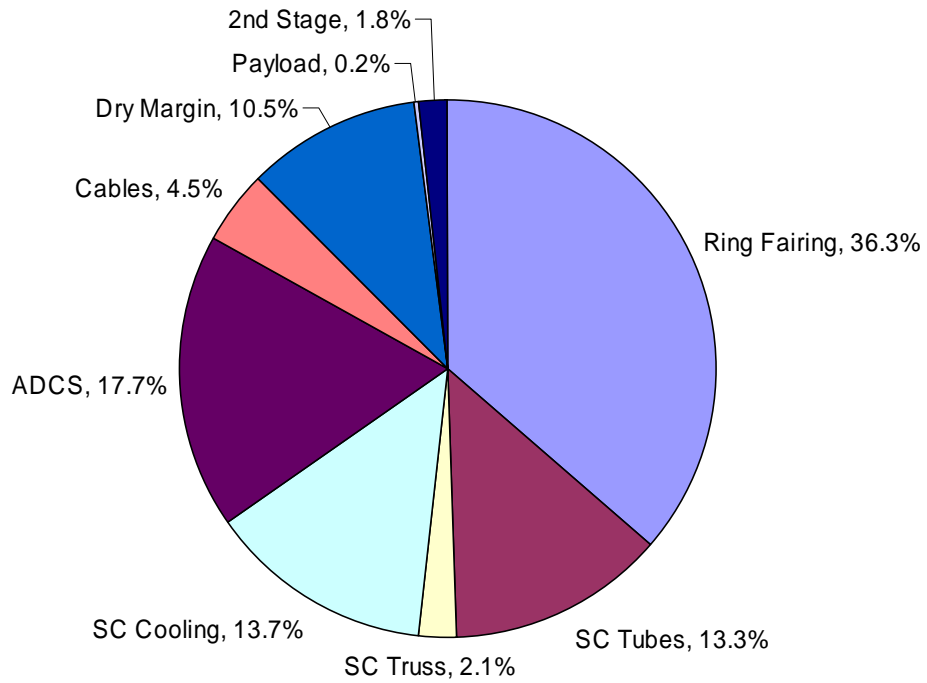**Figure 22: Weight breakdown for Magel infused with Nb₃Sn.**



**Figure 23: Weight breakdown for Magel infused with BSCCO.**

MCSs were then run on these three vehicles. The 50% confidence values are listed in Table 14 for each of the metrics. Assuming 20 flights per year for 30 years, these lead to costs per pound of $35,400 FY 2003/lbs, $35,700 FY 2003/lbs and $41,000 FY 2003/lbs for NbTi, Nb$_3$Sn and BSCCO respectively. NbTi is the most economically viable and feasible out of the three SC materials investigated. The other two materials have different tradeoffs but each one yields a final design that is more expensive than NbTi.

**Table 14: 50% confidence levels for the three MCSs. All dollar amounts are in FY 2003.**

| Metric | NbTi | Nb3Sn | BSCCO |
|---|---|---|---|
| Total DDT&E (B$) | 98.4 | 101 | 177 |
| TFU (B$) | 25.4 | 27.3 | 103 |
| Facilities Cost (B$/Site) | 43.6 | 43.9 | 50.0 |
| Fixed Operating Cost (B$/Year) | 28.3 | 28.3 | 28.3 |
| Variable Operating Cost (M$/Flight) | 62.6 | 62.6 | 62.8 |
| LCC (B$) | 1,210 | 1,220 | 1,400 |
| Cost per Pound to Orbit ($/lbs) | 35,400 | 35,700 | 41,000 |
| Gross Mass (MT) | 8,850 | 8,890 | 9,960 |
| Loss of Mission Reliability (MFBF) | 2250 | 2250 | 2242 |

## *Technology Sensitivities*

It is also useful to look at the effect that the individual technologies have on the vehicle. This will suggest which technologies to put development funds into. Each technology was individually applied to the baseline while the vehicle metrics were recorded. The new values for each metric were compared to the baseline values to find the amount that each changed by applying the technologies. The sensitivities for the vehicle's gross mass and LCC are shown in Figure 24 as well as in the Appendix.

Both SC materials induce a increase in both gross mass and LCC. This is mostly due to the fact that these materials increase the propulsion mass and that the propulsion subsystem is the driving component of the vehicle. On the other hand, all of the other technologies show a decrease in gross mass and LCC. This is because all of these technologies either decrease subsystem masses or decrease the current needed.
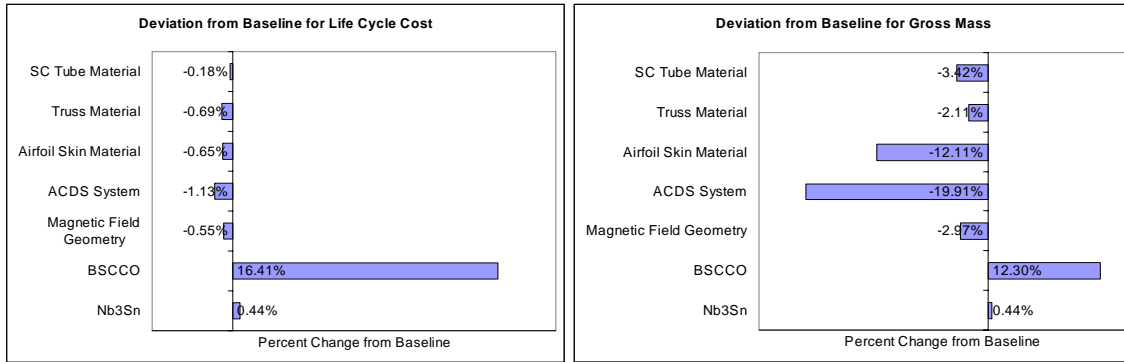
**Figure 24: LCC and gross mass sensitivity to each technology.**

# Conclusion

The Magel baseline was not viable and did not seem feasible. The vehicle cost too much and was too large with even the most conservative assumptions. By infusing technologies the vehicle became more and more viable and feasible. However, with the technologies considered, the vehicle was still not good enough.

The largest problem is the underlying physics of the architecture. The magnetic field from the ground station decreases too quickly with altitude and the geometry is unstable. Other geometries may prove to make the vehicle more efficient; most notably, eliminating the ADCS system from the launch vehicle and controlling the vehicle's movements completely from the ground.

Another good component to improve is the SC material choice or magnetic field geometry. These have the prospect to reduce the gross mass and cost considerably. NbTi, $Nb_3Sn$ and BSCCO are among the most commonly used SC materials due to their ability to handle large amounts of current and their relatively low cost. However, SC materials have not been considered for aerospace applications. Therefore, nobody has been concentrating on finding a SC material with low density. If a SC material is found with a high $J_c$ and low density then there is a greater prospect for the Magel architecture.

# References

1. Ham, C., et. al., "Maglifter: A Ground-Based Next Generation Reusable Launch Assist for a Low-Cost and Highly Reliable Space Access," 17th Annual/USU Conference on Small Satellites, SSC03-VIII-2, 2003.
2. Griffiths, D. J., "Introduction to Electrodynamics," 3rd ed. 1999, Prentice Hall.
3. Kinney, D. J., "CBAero 1.4 User's Guide," March 17, 2003.
4. Powell, J. R., Maise, G., Paniagua, J., "StarTram: A New Approach for Low-Cost Earth-to-Orbit Transport," IEEE, 0-7803-6599, February, 2001.
5. Olds, J. R., Class notes from AE 6320 at Georgia Institute of Technology, November 11, 2002.
6. Isakowitz, S. J., Hopkins, J. P., Hopkins, J. B., "International Reference Guide to Space Launch Systems," 3rd ed., AIAA, 1999.
7. Benson, T., "Earth Atmosphere Model," June 4, 2002, http://www.grc.nasa.gov/WWW/K-12/airplane/atmos.html.
8. Poole, C. P., Farach, H. A., Richard, J. C., "Superconductivity," Academic Press Inc., 1995.
9. Rohrschneider, R., "Development of a Mass Estimating Relationship Database for Launch Vehicle Conceptual Design," AE8900 Special Project, Georgia Institute of Technology, April 26, 2002.
10. Mannix, R., "Static Magnetic Field (0 Hz) Safety," University of California, EH & S.
11. "Magnetic Fields: Health and Safety Guide," World Health Organization, IPCS International Programme on Chemical Safety, Health and Safety Guide No. 27, 1989.
12. "Solids: Properties of Solid Materials," V3.5, CryoSoft, March 2002.
13. R. M. Scanlan, "Conductor Cost/Performance Status Report for Snowmass 2001," February 15, 2001.
14. Hart, P. B., et. al., "Microstructure, Impurity Content and Critical Current Density in $Nb_3Sn$," Journal of Applied Physics, April 1969.
15. Larbalestier, D. C., Hellstrom, E. E., "Applied Superconductivity Center: BSCCO," University of Wisconsin-Madison, http://www.asc.wisc.edu/bscco/bscco.htm, March 1, 2002.
16. Grant, P. M., Sheahen, T. P., "Cost Projections for High Temperature Superconductors," Applied Superconductivity Conference, September 1998.

# Appendix

## Deviation from Baseline for 1st Stage Diameter

| Category | Value |
|---|---|
| SC Tube Material | -1.69% |
| Truss Material | -3.39% |
| Airfoil Skin Material | -7.71% |
| ACDS System | -4.21% |
| Magnetic Field Geometry | -2.44% |
| BSCCO | 16.13% |
| Nb3Sn | 0.61% |

Percent Change from Baseline

## Deviation from Baseline for 1st Stage Peak Velocity

| Category | Value |
|---|---|
| SC Tube Material | -0.002% |
| Truss Material | -0.006% |
| Airfoil Skin Material | 0.049% |
| ACDS System | -0.062% |
| Magnetic Field Geometry | -2.252% |
| BSCCO | -0.006% |
| Nb3Sn | 0.001% |

Percent Change from Baseline

**Deviation from Baseline for Loss of Mission Reliability**

| | Percent Change from Baseline |
|---|---|
| SC Tube Material | 0.000017% |
| Truss Material | 0.000033% |
| Airfoil Skin Material | 0.000089% |
| ACDS System | 0.000029% |
| Magnetic Field Geometry | -0.000470% |
| BSCCO | -0.000166% |
| Nb3Sn | -0.000006% |



**Deviation from Baseline for DDT&E**

| | Percent Change from Baseline |
|---|---|
| SC Tube Material | -0.85% |
| Truss Material | -3.89% |
| Airfoil Skin Material | -6.90% |
| ACDS System | -5.30% |
| Magnetic Field Geometry | -2.92% |
| BSCCO | 74.69% |
| Nb3Sn | 2.06% |

**Deviation from Baseline for TFU**

| Category | Percent Change from Baseline |
|---|---|
| SC Tube Material | -2.70% |
| Truss Material | -4.43% |
| Airfoil Skin Material | -20.36% |
| ACDS System | -6.29% |
| Magnetic Field Geometry | -3.50% |
| BSCCO | 278.09% |
| Nb3Sn | 6.68% |

**Deviation from Baseline for Facilities Cost**

| Category | Percent Change from Baseline |
|---|---|
| SC Tube Material | -0.34% |
| Truss Material | -3.26% |
| Airfoil Skin Material | 0.43% |
| ACDS System | -5.56% |
| Magnetic Field Geometry | -3.17% |
| BSCCO | 13.49% |
| Nb3Sn | 0.66% |

**Deviation from Baseline for Fixed Cost per Year**

| Category | Percent Change from Baseline |
|---|---|
| SC Tube Material | 0.003% |
| Truss Material | -0.003% |
| Airfoil Skin Material | 0.866% |
| ACDS System | -0.001% |
| Magnetic Field Geometry | -0.006% |
| BSCCO | -0.028% |
| Nb3Sn | -0.001% |

**Deviation from Baseline for Cost per Flight**

| Category | Percent Change from Baseline |
|---|---|
| SC Tube Material | -0.071% |
| Truss Material | -0.044% |
| Airfoil Skin Material | -1.06% |
| ACDS System | -1.62% |
| Magnetic Field Geometry | 0.22% |
| BSCCO | 0.39% |
| Nb3Sn | 0.014% |